

Examination of experimental errors in Scanlan derivatives of a closed-box bridge deck

Fabio Rizzo^{1,2a} and Luca Caracoglia^{*1}

¹Department of Civil and Environmental Engineering, Northeastern University, Boston, MA 02115, USA

²Department of Engineering and Geology, University "G. D'Annunzio", Pescara, PE 65127, Italy

(Received November 28, 2017, Revised March 2, 2018, Accepted March 8, 2018)

Abstract. The objective of the investigation is the analysis of wind-tunnel experimental errors, associated with the measurement of aeroelastic coefficients of bridge decks (Scanlan flutter derivatives). A two-degree-of-freedom experimental apparatus is used for the measurement of flutter derivatives. A section model of a closed-box bridge deck is considered in this investigation. Identification is based on free-vibration aeroelastic tests and the Iterative Least Squares method. Experimental error investigation is carried out by repeating the measurements and acquisitions thirty times for each wind tunnel speed and configuration of the model. This operational procedure is proposed for analyzing the experimental variability of flutter derivatives. Several statistical quantities are examined; these quantities include the standard deviation and the empirical probability density function of the flutter derivatives at each wind speed. Moreover, the critical flutter speed of the setup is evaluated according to standard flutter theory by accounting for experimental variability. Since the probability distribution of flutter derivatives and critical flutter speed does not seem to obey a standard theoretical model, polynomial chaos expansion is proposed and used to represent the experimental variability.

Keywords: long-span bridges; Scanlan (flutter) derivatives; wind tunnel tests; bridge flutter; experimental error analysis; probability estimation; polynomial chaos expansion

1. Introduction

The dynamic response prediction for long-span bridges, exposed to wind loads, is a complex task. The study of bridge flutter has attracted the attention of the scientific community because of the susceptibility to flutter-induced catastrophic bridge failure. Over the years, analytical and numerical methods have been developed and successfully applied to the quantification of the loads and the simulation of the response (Scanlan and Tomko 1971, Huston *et al.* 1988, Jain 1996, Jain *et al.* 1996, Katsuchi *et al.* 1999, Gu *et al.* 2001, Kim *et al.* 2004, Sharan *et al.* 2008, Starossek *et al.* 2009). However, it remains necessary to perform physical experiments to gain critical information for the analysis of the fluid-flow forces on bridge decks. Among the various studies, the use of probability-based analysis to study flutter occurrence has been considered (e.g., Cheng *et al.* 2005, Ge *et al.* 2000, Pourzeynali and Datta 2002, Dragomirescu *et al.* 2003, Mannini and Bartoli 2007). Probabilistic methods are necessary to investigate bridge stability and the ultimate limit state associated with flutter.

These methods, often based on stochastic calculus (Grigoriu 2002), are also employed to examine the effects of atmospheric turbulence on flutter onset (e.g., Lin and

Ariaratnam 1980, Bucher and Lin 1988, Sarkar and Tsiatas 2009, Bartoli *et al.* 1997, Cai and Albrecht 2000, Sepe and D'Asdia 2003, Sepe and Vasta 2014) and beyond flutter, i.e., in a post-critical state (e.g., Hračov *et al.* 2005, Náprstek and Pospíšil 2004, Pospíšil *et al.* 2006).

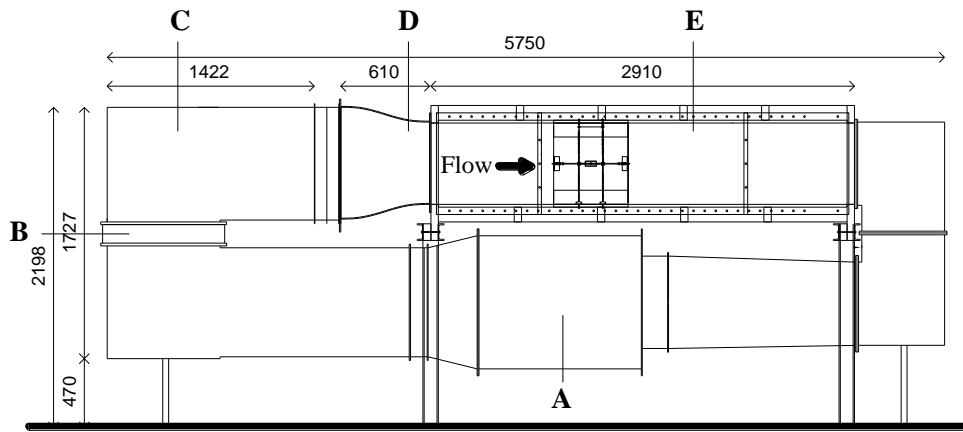
In recent years, analysis models have also been proposed to investigate the effect of various sources of uncertainty (modeling simplifications, experimental errors, etc.) on flutter onset, either by using a collection of samples acquired in repeated wind tunnel tests on a section model of a bridge deck (e.g., Brito and Caracoglia 2009, Seo and Caracoglia 2012, Baldomir *et al.* 2013a, b) or by simulating the problem of uncertainty propagation through the addition of random error terms and suitable perturbation of the aeroelastic deck loads (e.g., Caracoglia 2013, Canor *et al.* 2015). Further examination of recent experimental studies on aeroelastic loads for bridge decks (Sarkar *et al.* 2009, Kwon 2010, Argentini *et al.* 2014) confirms that uncertainty evaluation is necessary while conducting an experiment to determine the aeroelastic loads (flutter derivatives). Information about load variability, such as tolerance intervals of the flutter derivatives, should possibly be included in flutter predictions. The consideration of experimental uncertainty might in turn lead to more accurate estimation of flutter probability, for example through Monte Carlo sampling methods (e.g., Xu 2013). Specific experimental studies are consequently needed to analyze variability in the flutter derivatives, determined from wind tunnel tests and any effects on the prediction of the structural response. This topic is not only relevant to the wind engineering community but also to the more

*Corresponding author, Associate Professor

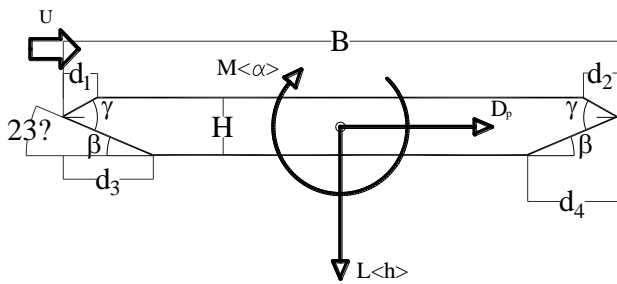
E-mail: lucac@coe.neu.edu

^a Ph.D.

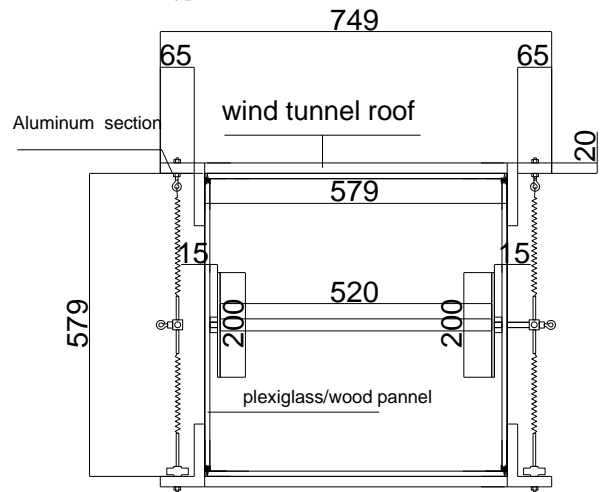
E-mail: fabio.rizzo@unich.it



(a) Wind tunnel test chamber schematic (lateral/longitudinal view) [(A) motor/fan (11.2 kW), (B) air cooling system, (C) settling chamber, (D) convergent, (E) test chamber (600 x 600 mm cross-section)]



(b) Cross section details of the deck models [aeroelastic forces per unit length and degrees of freedom, according to Scanlan's sign convention and notation, are also reported]



(c) Schematic drawing of test chamber cross-section and experimental rig [measurements in millimeters]



(d) Photograph of the test rig (leeward cross-section)



(e) Longitudinal view of the test chamber and setup

Fig. 1 Schematics of the test rig

general field of aeroelasticity (e.g., Khalil *et al.* 2016).

This paper summarizes the results of an experimental study motivated by the need for “more accurate” measurement of self-excited forces for bridge decks in wind tunnel.

The hypothesis is that, if a large sample of data is available (e.g., by repeating the experiments needed to extract the flutter derivatives), errors linked to the estimation of aeroelastic loads can be studied. For this purpose, a test rig for wind tunnel tests of bridge section

models (Fig. 1(a)), using a two-DOF (degree of freedom) spring-supported apparatus and built at Northeastern University (NEU), is employed. As a first example, the flutter derivatives of one section model were determined. The model corresponds to an example of closed-box girder section.

The paper investigates the variability of a set of repeated acquisitions and identifications of flutter derivatives by free-vibration method, attributed to the effects of measurement errors and imperfect laboratory conditions. The variability in the experimental values of the flutter derivatives is subsequently used to predict, in a probabilistic setting, the coupled flutter instability of the wind tunnel model. The critical flutter speed of the setup is evaluated according to standard flutter theory by accounting for variability in the flutter derivatives. Since the probability distribution of flutter derivatives and critical flutter speed does not seem to obey a standard theoretical model, Polynomial Chaos expansion (Ghanem and Spanos 1991, Xiu and Karniadakis 2002) is also proposed and employed to represent the experimental variability. Hermite polynomials are investigated to enable the stochastic analysis. Even though the nonlinear transformation of random variables, exploiting orthogonal Hermite polynomials, has been considered in wind engineering, for example for the study of unsteady pressure fields in wakes or turbulence regions of structures (e.g., Gurley and Kareem 1997), this approach has seldom been examined in the context of bridge aeroelasticity.

This type of investigation is also important for understanding the fidelity of the experimental data and to evaluate the dependence between the sample data, acquired experimentally, and the structural parameter used to design. Furthermore, even though relevance of variability in the experimental flutter derivatives is widely reported in the literature, no standard examination protocols are available.

2. Background

The dynamic response of a long-span bridge due to wind excitation can be modeled through the multi-mode approach in the frequency domain. The dynamic component of the wind loading, causing deck vibration, can be represented by superposition of turbulence-induced (buffeting) forces and motion-induced (aeroelastic) forces. Self-excited forces, acting on a unit-length section of the deck (Fig. 1(b)), are defined as lift (L_h), drag (D_p) and moment (M_α). These forces are commonly based on a first-order linear expansion of the h vertical displacement and α torsional rotation of the generic deck cross section, first introduced by Scanlan and Tomko (1971). The effects the lateral DOF and D_p , usually important in special cases only (e.g., Katsuchi *et al.* 1999), were not considered. Even though this model is strictly valid for simple-harmonic vibration of the deck, it is usually acceptable for small-amplitude random vibration. Consequently, the aeroelastic lift and moment forces of the generic cross section, per unit deck span (or longitudinal model length), were determined as reported in Eqs. (1).

$$L_h = \frac{1}{2} \rho U^2 B \left[KH_1^*(K) \frac{\dot{h}}{U} + KH_2^*(K) \frac{B\dot{\alpha}}{U} + K^2 H_3^*(K) \alpha + K^2 H_4^*(K) \frac{h}{U} \right] \quad (1a)$$

$$M_\alpha = \frac{1}{2} \rho U^2 B^2 \left[KA_1^*(K) \frac{\dot{h}}{U} + KA_2^*(K) \frac{B\dot{\alpha}}{U} + K^2 A_3^*(K) \alpha + K^2 A_4^*(K) \frac{h}{U} \right] \quad (1b)$$

In the previous equations ρ is the air density, U the mean wind speed perpendicular to the bridge (or model) longitudinal axis, B is the deck width; the “over-dot” symbol denotes derivation with respect to time t . The quantities H_i^* and A_i^* (with $i=1, \dots, 4$) are the “Scanlan or flutter derivatives” (Scanlan and Tomko 1971). These functions are experimentally found in wind tunnel by testing a section model of the full-scale girder at a reduced scale. The flutter derivatives depend on the reduced frequency $K=\omega B/U$ or, equivalently, reduced velocity $U_r=U/(nB)=2\pi/K$, with ω being the angular vibration frequency of the deck in rad/s and $n=\omega/(2\pi)$ the frequency in Hz. The dynamic equilibrium equations of the 2-DOF system (Fig. 1(b)), which is tested in the wind tunnel, reproduce the vertical (h) and torsional (α) aeroelastic vibration of a representative finite-length section of the full-scale bridge deck. The lift force L_h and overturning moment M_α per unit length of the deck are measured over the span length ℓ of the experimental model. The dynamic equations [Eq. (2)] of the 2-DOF system, reproducing the vibration of the apparatus tested in wind tunnel, can be derived as shown below, following the original formulation by Scanlan and Tomko (1971), reported in Simiu and Scanlan (1986).

$$M \left(\ddot{h} + \ddot{\alpha} \frac{S}{M} + 2\zeta_h \omega_h \dot{h} + \omega_h^2 h \right) = L_h \ell, \quad (2a)$$

$$I_\alpha \left(\ddot{\alpha} + \ddot{h} \frac{S}{I_\alpha} + 2\zeta_\alpha \omega_\alpha \dot{\alpha} + \omega_\alpha^2 \alpha \right) = M_\alpha \ell \quad (2b)$$

In Eqs. (2) M is the total mass of the model over the length ℓ , which also accounts for the mass of the moving components of the experimental rig; I_α is the total mass moment of inertia; S is the static mass unbalance about the elastic axis, equal to the product of mass M and the distance (with appropriate sign) between the elastic center (center of stiffness) and the center of mass; ℓ is the longitudinal length of the model; ω_h and ω_α are the angular frequencies of vibration corresponding to the two DOFs; ζ_h and ζ_α are the corresponding structural damping ratios. The damping ratio coefficients replicate unavoidable dissipation mechanisms in the wind tunnel setup, which cannot be eliminated. The careful selection of the model’s frequencies is also an important issue in the design of the experimental apparatus to ensure the successful measurement of the flutter derivatives.

After the experimental measurement of the flutter derivatives, Eq. (2) was used to determine the critical flutter speed of the model, tested in the wind tunnel. The solution to the flutter problem was based on the original 2-DOF flutter theory, proposed by Scanlan. Calculation of the flutter speed was based on the iterative procedure described by Simiu and Scanlan (1986), simulating a 2DOF dynamical system with mass, inertia, damping ratios and

flutter derivatives corresponding to the actual setup.

3. Description of the experiments

3.1 Aeroelastic force balance

Experimental tests were conducted in the closed-circuit small-scale wind tunnel of NEU. The tunnel has a test section with transverse dimensions of 559 mm × 559 mm (Fig. 1(a)). The motor/fan can produce steady airflow speeds up to about 20 m/s without turbulence. A newly-designed aeroelastic balance was used for the aeroelastic tests. The design was based on a previous experimental apparatus, developed for a smaller test section (Brito and Caracoglia 2009, Seo and Caracoglia 2012). The experimental setup has two DOFs: vertical h , and torsional α . The design included an H-shaped rig for the suspension of the model (one on each side of the model), which can be vertically supported through a set of extension springs. The spring properties were selected to produce the desired stiffness (i.e., angular frequencies ω_h and ω_α). The distance between the two vertical supports and the springs, equal to 139.7 mm, was found after calibration to maintain an adequate frequency ratio between the vertical and torsional modes (DOFs h and α).

Fig. 1(b) illustrates the model cross-section, whereas Fig. 1c shows the schematics of the setup. Figs. 1(d) and 1(e) show internal views of the wind tunnel during the execution of the tests. The first photograph is taken looking from the leeward side of the section model, also noticeable in its suspended position in the middle of the chamber. Fig. 1(e) shows a longitudinal view of the test chamber.

Dimensions of the force balance components, H-shaped rig, suspension system with extensions springs and the optimal location of the section model can be seen in both Figs. 1(a) and 1(c). The lateral horizontal DOF and other undesired motions were restricted by means of pre-tensioned piano-wires, connected to aluminum L-shaped profiles, anchored outside the test chamber in the proximity of the horizontal middle section. This configuration restricts all the horizontal DOFs, both in the direction of the drag force (D_p) and in the transverse direction corresponding to the longitudinal bridge model axis, but permits free vibration in the vertical direction and rotation about the center point of the rig. The system of cables and restrainers was initially tested to ensure that undesirable effects (e.g., nonlinearity induced by the pre-tensioned cables) were not significant.

The free-vibration method (Scanlan and Tomko 1971) was employed for the extraction of the flutter derivatives. Experiments did not consider the use of the forced-vibration method (e.g., Matsumoto 1996, Matsumoto *et al.* 1996, Matsumoto *et al.* 1998, Sato *et al.* 2004). Description of both measurement methods may be found in Sarkar *et al.* (2009).

The time histories of the free-decay displacements h and α were derived from the instantaneous force measurements recorded by three load cells, placed outside the test chamber at selected support anchorages (Fig. 1(c)). In the free-decay

tests the repeatability of the initial motion conditions (normalized initial amplitudes h_0/B and α_0), imposed to the aeroelastic model, was an important issue. Initial motion conditions were selected to allow for both 1-DOF and 2-DOF aeroelastic tests ($h_0 \neq 0$ with $\alpha_0 = 0$; $h_0 \neq 0$ and $\alpha_0 \neq 0$). The forthcoming results are primarily derived from the 2-DOF tests.

3.2 Section model, wind tunnel setup and preliminary experiments

The section model tested was designed for the specific purposes of this experiment as a typical example of closed-box girder of a modern long-span bridge. The dimensions of the section model are reported in Table 1; the model features and the direction of the aeroelastic forces and DOFs are also schematically illustrated in Fig. 1(b).

The model length ℓ was 533.4 mm. The model dimensions were also chosen to limit the blockage effect in the chamber. This effect was estimated as less than 1% and was therefore negligible. The mean flow speed was varied in the wind tunnel between 2 m/s and 9 m/s (Table 2); in the same table the reduced velocity U_r , based on the vibration frequency of the vertical DOF, is also shown. This reduced velocity (U_r) was found from U and B and later used to plot the experimental results after extraction of the flutter derivatives.

At each speed 30 repeated experiments and free-decay motion acquisitions were performed to obtain a sufficiently large sample of data and to study the variations in the flutter derivatives.

The number of tests was selected from previous experience (Brito and Caracoglia, 2009, Seo and Caracoglia, 2012), keeping in mind that many repeated acquisitions were impractical and difficult to carry out in the laboratory.

Table 1 Geometric properties and dimensions of the bridge section model

d_1	d_2	d_3	d_4	B	H	θ	β
[mm]	[mm]	[mm]	[mm]	[mm]	[mm]	[°]	[°]
12	12	32	32	148	20	30	23

Table 2 Wind tunnel flow speeds and reduced velocities

U [m/s]	1.90	2.64	3.38	4.25	5.30	6.26	7.43	8.40
U_r	3.28	4.57	5.86	7.36	9.18	10.86	12.89	14.56

Table 3 Physical properties of the bridge section models

Quantity	Symbol	Units	Value assigned
Mass per unit length	m	kg m ⁻¹	2.743
Mass moment of inertia per unit length	I	kg m ² m ⁻¹	0.010
Vertical-DOF frequency (h)	$\omega_h/2\pi$	Hz	3.89
Torsional-DOF frequency (α)	$\omega_\alpha/2\pi$	Hz	6.78
Frequency ratio, ω_α/ω_h	ε	-	1.74

For each acquisition, the flutter derivatives were independently evaluated and used for error analysis. Variations in the flutter derivatives were later investigated at each flow speed.

3.3 Preliminary examination of the experimental data

An example of the acquired time history is reported in Figs. 2(a) and 2(b), for a wind speed of about 5 m/s. The figures illustrate two typical experiments, conducted respectively using 1-DOF and 2-DOF free-decay tests; the vertical-DOF values are normalized as h/B . Time histories of the responses h, α were indirectly found from the measurements of the reaction forces in the load cells located in correspondence with the anchorages of the support springs in Fig. 1(c). Forces were converted to displacement and rotation by suitable calibration of the apparatus. Details are omitted but explanation may be found in Brito and Caracoglia (2009).

In Figs. 2(b) and 2(d) the data of the torsional DOF are exclusively shown in the case of 2-DOF example experiment; coupling between the h and α motions is evident (Fig. 2(d)). In these figures, the original signal, acquired by the aeroelastic force balance and labeled as “raw data” in the graphs, is compared to the signal obtained after applying a band-pass digital filter, labeled as “filtered data”. A Butterworth digital filter was used to remove high frequency disturbances (instrumental noise above 12 Hz) without compromising the fidelity of the data at low frequencies. The same procedure of preliminary low-pass filtering is recommended by the developers of the flutter derivative identification algorithm (Chowdhury and Sarkar 2003, 2004), which is later discussed in Section 4.1. In the graph of Fig. 2(d) the signal is also filtered to isolate the contribution of the torsional vibration from the vertical vibration.

The graphs exclusively show the time histories of the free-vibration decay immediately after the system’s release. In this example, the time histories correspond to a typical experiment with the highest wind tunnel speed considered (Table 2). Due to a dominant “damping effect”, provided by the aeroelastic loads, the torsional motion rapidly fades, almost imperceptible by visual inspection of the time histories, whereas the vertical vibration persists for about 3 s. For each acquisition, the Power Spectral Density (PSD) is also presented to identify the main frequency components of each signal. This type of graphs was employed to qualitatively confirm that, after post-processing the raw data by digital filter, important information was not removed from the original data. In the PSD graphs shown in Figs. 2(c) and 2(d), respectively for 1DOF and 2DOF tests, it is observed that, as reported in Table 3, the ratio between torsional and vertical frequency is about 1.7. Finally, the filtered data were analyzed to possibly detect irregular trends in the free-decay time histories and anomalies in the experimental procedure, such as small imperfections or misalignments in the setup. Vibration amplitude effects in the flutter derivatives, which are possible in the case of bluff deck sections (e.g., documented by Sarkar *et al.* 2009), were not directly considered; any influence was

incorporated (i.e., interpreted) as experimental error or variability. Preliminary data records, for example presented in Figs. 2(a) and 2(b), revealed no unexpected large irregularity, potentially linked to a systematic error.

It was also important to investigate the possible variability in the initial motion conditions, imposed before the release of the system. One of the main concerns of the investigation, which relied on the repetition of several similar experiments, was to retain the same initial conditions from one test to another. As an example, Fig. 3a and Fig. 3(b) examine the initial motion conditions before release of the model at various reduced velocities in dimensionless form, vertical (h/B) and torsional (α); information was derived from the collection of the thirty 2-DOF repeated experiments at each U . The initial values were indirectly found by inspection of the data sets and by using the results of the Shannon reconstruction formula, described in a later section. The figures are “box-and-whisker” plots of h/B and α ; it is shown that the median initial displacement is approximately preserved as U varies (approximately 0.05 for the normalized initial displacement and 0.15 for the rotation). The variability is, however, not insignificant since the inter-quantile range may on occasion be of the same order as the median value, especially for h/B (for example at $U_r=4.57$ in Fig. 3(a)). In general, repeated setting of initial conditions was better achieved with the rotational DOF, since more uniformity and smaller variations are noticeable in Fig. 3(b). Moreover, Fig. 3 also suggests that initial conditions do not strongly depend on wind speed and the various experiments. Therefore, the observed variability could be treated as part of the experimental procedure and examined in the context of error analysis.

Finally, one important aspect during the experiments was the derivation of the reference damping ratios of the moving setup (ζ_h and ζ_α) in the absence of airflow; more discussion is presented in the next section.

4. Analysis of experimental results

4.1 Background: identification of flutter derivatives

Flutter derivatives were derived from the measurement of the vertical- and torsional-DOF free decay time histories at various airflow speeds. Various methods can be used to identify the flutter derivatives. For example, Qin and Gu (2004) and Mishra *et al.* (2006) proposed the use of a covariance-driven Stochastic Subspace Identification technique (SSI). Recently, Zhu and Gu (2014) identified flutter derivatives using CFD-based discrete-time aerodynamic models.

In this study, the identification method used is the Iterative Least Squares (ILS) method, developed by Chowdhury and Sarkar (2003 and 2004), which was later utilized by Chen *et al.* (2002, 2006). The ILS method relies on a state-space formulation of the 2-DOF dynamic problem, as concisely described in Eqs. 3(a) and 3(b) below.

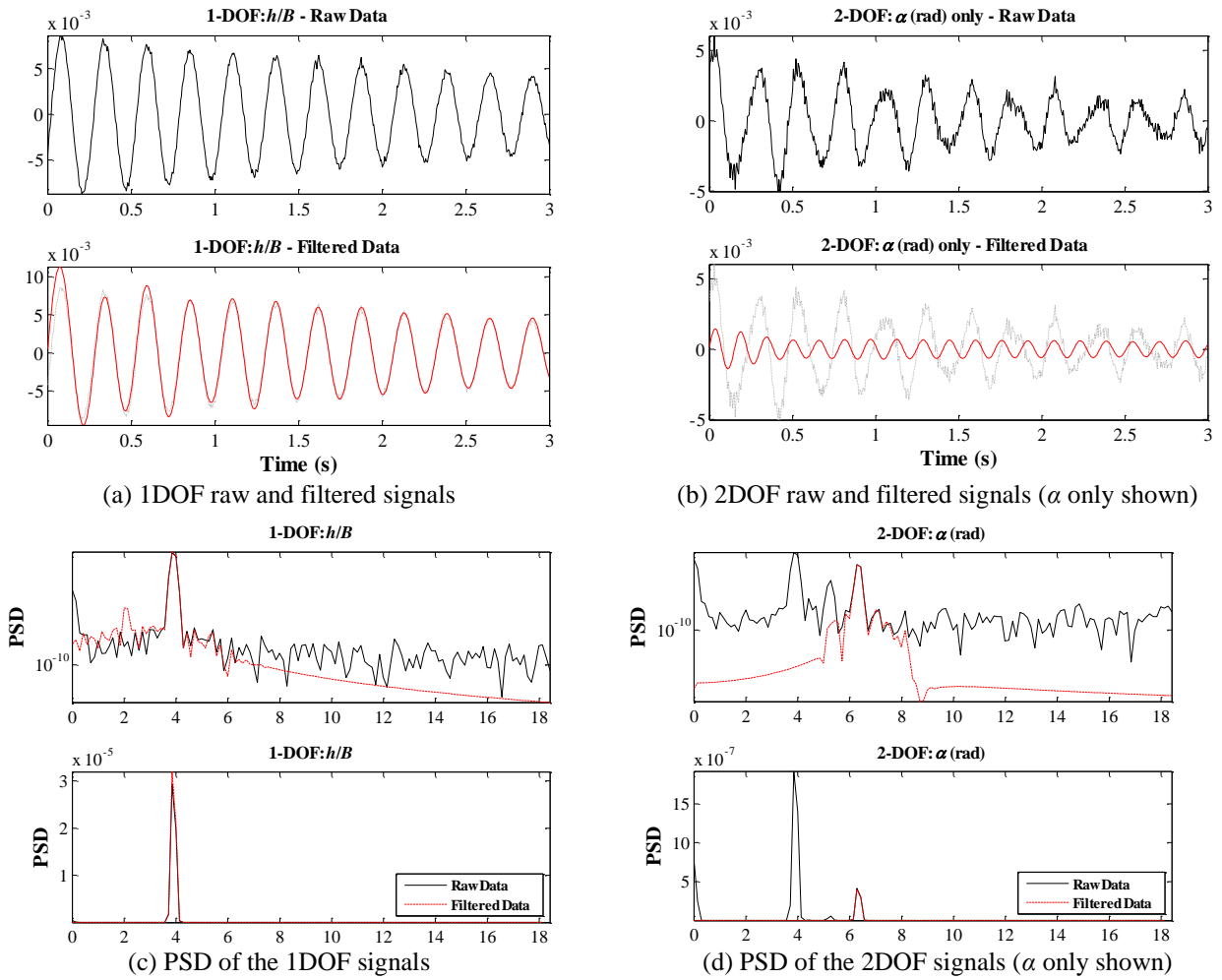


Fig. 2 Example of wind tunnel signal analysis (1DOF and 2DOF free-decay experiments)

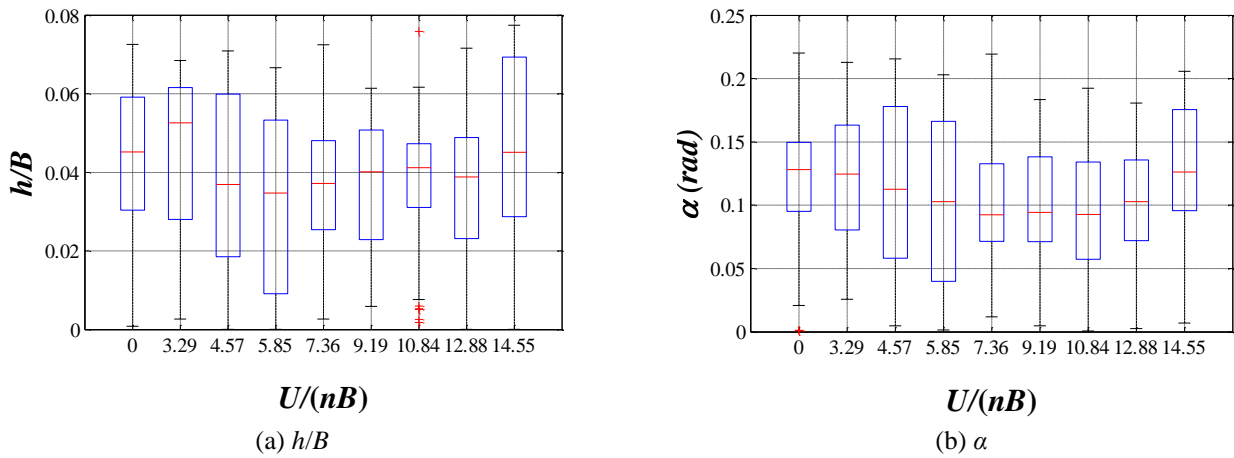


Fig. 3 Examination of the initial motion conditions and their variability at the release of the model

A brief overview of the method is provided below for the sake of completeness. The ILS employs the state column vector of the motion variables $\underline{Z} = [h, \alpha, \dot{h}, \dot{\alpha}]^T$ (with T denoting transpose operator) and transforms the dynamic equations of motion, which include the effect of the fluid-structure interaction, into a linear dynamical system (Chowdhury and Sarkar 2003, 2004).

$$\dot{\underline{Z}} = \underline{A}\underline{Z}, \quad (3a)$$

$$\underline{A} = \begin{bmatrix} 0 & I \\ -\underline{K}^{eff} & -\underline{C}^{eff} \end{bmatrix}. \quad (3b)$$

In Eqs. (3), the vector \underline{Z} contains displacement and velocity data for each DOF and \underline{A} is the state matrix. The sub-matrices \underline{K}^{eff} and \underline{C}^{eff} are equivalent (i.e., generalized) stiffness and damping matrices, which can be directly related to flutter derivatives in Eq. (1). The contribution of the mass and inertia of the vibrating model/setup is accounted for in Eqs. (3). For more information on the ILS method, the reader is referred to Chowdhury and Sarkar (2003).

Flutter derivatives, which are usually plotted as a function of the reduced velocity $U_r = U/(nB)$, can be extracted from the identification of \underline{K}^{eff} and \underline{C}^{eff} during wind tunnel tests at a given speed U ("wind-on" test). The ILS method operates by iteratively finding the terms of \underline{K}^{eff} and \underline{C}^{eff} by using the measurement of h, α and the numerical estimation of $\dot{h}, \dot{\alpha}$ and $\ddot{h}, \ddot{\alpha}$.

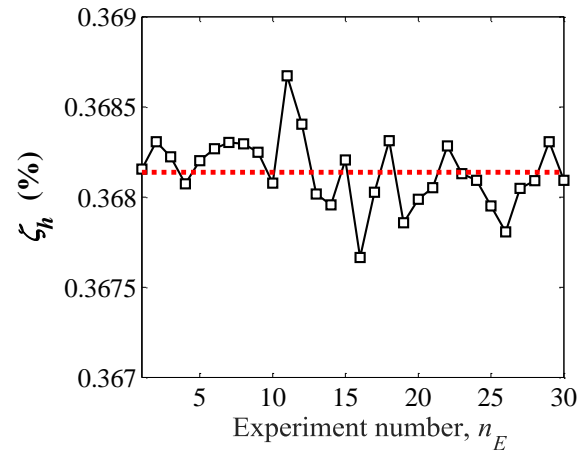
The flutter derivatives were found by direct comparison of the elements in \underline{K}^{eff} and \underline{C}^{eff} against the same elements obtained from a reference test in the absence of airflow ("wind-off" test). The latter experiments were also useful to determine the properties of the setup, such as ζ_h and ζ_α ; estimation of the mass and moment of inertia of the moving setup is also needed for the calculation of the derivatives [refer to Eqs. (4) and (5) in Chowdhury and Sarkar (2003)]. The experimental sampling rate (200 samples/s) was selected to enable the measurement of h, α and the identification of the parameters from the elements of matrix \underline{A} . Since the first and second derivatives of h, α with respect to time are not measured, they need to be numerically estimated to apply the ILS procedure; in this work and contrary to Chowdhury and Sarkar (2003, 2004) the quantities $\dot{h}, \dot{\alpha}$ and $\ddot{h}, \ddot{\alpha}$ were estimated by application of the Shannon reconstruction formula (Jerri 1977).

The test procedure also requires the estimation of m and I (or $M = m\ell$ and $I_\alpha = I\ell$), which are not known since they include the influence of the moving parts of the apparatus. These quantities can be determined by conducting a set of preliminary experiments and monitoring the changes in the vibration frequencies consequent to the addition of supplementary concentrated masses of known mass and moment of inertia on the support bars of the rig. This operation was derived by adaptation of the procedure described by Sarkar (1992); the values of m and I are also shown in Table 3 for the section model (Fig. 1(b)) under consideration.

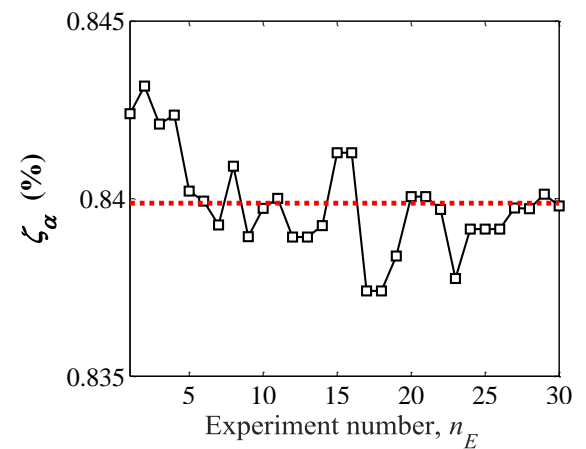
Figs. 4(a) and 4(b) illustrate the results of the initial wind-off tests used to determine the mechanical damping ratios of the vertical-DOF and torsional-DOF. Repetition of the tests was also employed in this case to further examine irregular dynamic behavior in the setup before investigating the aeroelastic loads. The values of ζ_h and ζ_α are plotted in each panel for each acquisition (experiment number, n_E). The mean values, indicated by a dashed line in the figure, were estimated from the sample as equal to 0.36% and 0.85%. As shown in Fig. 4, the variability in the damping ratios is relatively small compared to the mean values (less than one percent for both DOFs), suggesting that the experimental setup and procedure in the absence of wind flow in the chamber, was reliable and adequate for the subsequent measurement of the flutter derivatives.

4.2 Examination of flutter derivatives – mean graphs

In Figs. 5 and 6 the flutter derivatives are presented, respectively H_i^* and A_i^* with $i=1, \dots, 4$. In each panel of the two figures the mean graph is plotted as a solid continuous line with markers; the mean graph is found by computing the sample average at each U_r .



(a) Mechanical damping ratio ζ_h



(b) Mechanical damping ratio ζ_α

Fig. 4 Mechanical damping ratios ζ_h and ζ_α (percentage with respect to critical value) derived from the repeated experiments in the absence of airflow

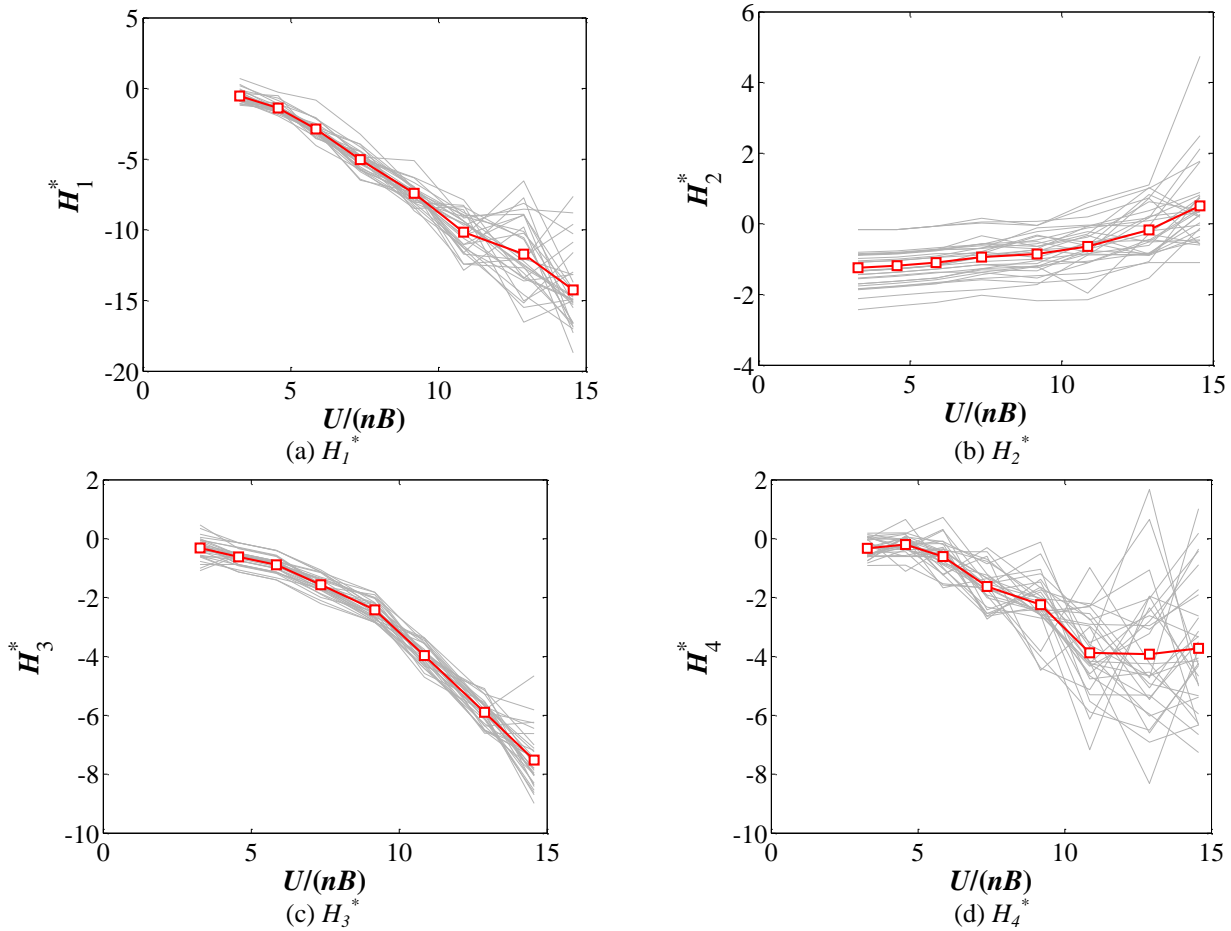


Fig. 5 Variability in the flutter derivatives, derived by examining the results of the expected experiments (lift force)

Moreover, plots of each of the thirty independent realizations are also overlapped, reduced velocity by reduced velocity, which were obtained by repeatedly applying the ILS procedure to each acquisition and U_r . This operation resulted in a total of thirty curves, “scattered” around the mean graph, found by connecting two adjacent data points at various U_r . These curves are also shown in the figures as light-colored continuous thin lines. The mean graphs of the flutter derivatives, presented in Figs. 5 and 6, seem compatible with the geometry of the selected closed-box girder (Fig. 1(b)) even in comparison with similar closed-box deck girders. Small negative values can be seen for A_2^* at low U_r .

4.3 Estimation of flutter speed by using the mean flutter derivatives

Using the mean values of the derivatives at each reduced velocity, the mean flutter condition was determined. Calculation of the flutter speed in this section and subsequent ones was based on the iterative procedure described by Simiu and Scanlan (pages 231-234, 1986) for a 2DOF dynamical system, with mass, inertia, damping ratios and flutter derivatives corresponding to the actual setup. The flutter condition was iteratively found by varying the reduced frequency $K=2\pi nB/U=2\pi/U_r$ [with $U_r=U/(nB)$

reduced velocity, previously defined] and by estimating the coupled-flutter angular frequency (ω_c) until convergence of the method. The mean values of the critical wind speed (U_c) and the critical flutter angular frequency (ω_c) were determined.

The predicted mean value of ω_c is equal to 37.82 rad, whereas the mean U_c is equal to 33.64 m/s for the 2DOF section model of this bridge. During the experiments the system was not driven to large flow speeds, closer to the flutter onset, to prevent damage to the setup. For this reason, increased oscillation was not observed in wind tunnel. Additional investigation on flutter speed viability is presented in a subsequent part of this paper.

5. Examination of data variability and experimental errors

Figs. 5 and 6 present the various graphs of the derivatives.

It is possible to note in the figures that all the curves (continuous thin lines without markers) are fairly close to the mean graph, except for the high U_r where a larger deviation from the mean can be seen. This behavior is believed to be caused by a more problematic control of the regular free-decay vibration in the experimental chamber at

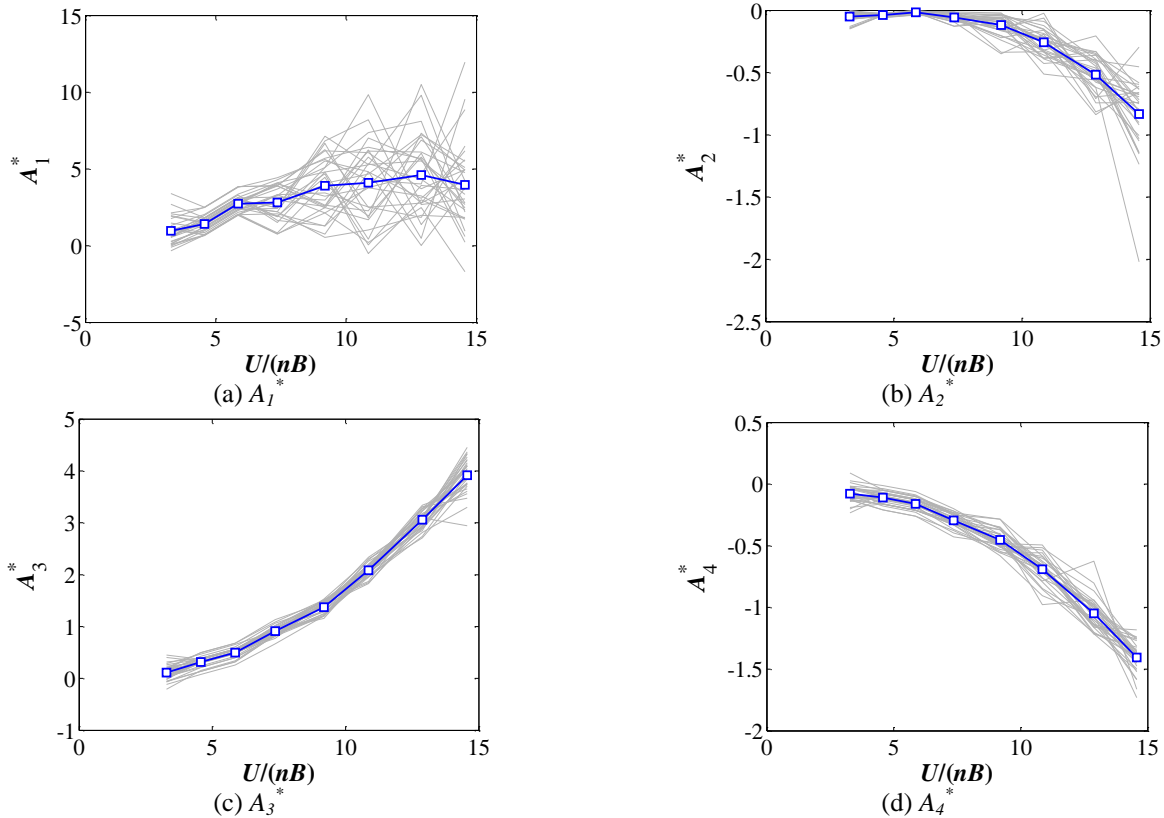


Fig. 6 Variability in the flutter derivatives, derived by examining the results of the expected experiments (torsional moment)

high speeds, which becomes more susceptible to external disturbances (such as small turbulence or test imperfections). This limitation is typical of the free-vibration method for the extraction of the flutter derivatives, as reported by several investigators (e.g., Sarkar *et al.* 2009).

The variability in the flutter derivatives is one of the objectives of the study; it is well captured in Figs. 5 and 6. The fundamental proposition, used to explain the observed variations, is the experimental error in a general sense. Errors are due to several issues, for example some variability in initial motion conditions imposed during each repetition of the tests (Fig.3), the unavoidable imperfections in the test setup, “environmental conditions” of the laboratory, etc. Each experiment was considered as an independent realization of a stochastic process at each reduced velocity U_r . Therefore, it is relevant to document the statistical moments (standard deviation, etc.) and to possibly examine the probability distribution from the data in this investigation.

5.1 Statistical moments of the error-contaminated flutter-derivatives

In Figs. 7 and 8 the standard deviation (σ) and the coefficient of variation (γ), used to study the dispersion of the sample distribution, are plotted as function of the reduced velocity. The quantity γ is equal to $\sigma/|\mu|$ with μ equal to the mean value.

It can be observed (Figs. 8 and 9) that the standard deviation of the error in the flutter derivatives increases

with the flow speed. The reason is that the control of experimental conditions is less repeatable at higher speeds and the experimental setup is likely to be affected by secondary undesirable motion, as outlined earlier. A secondary undesirable (rotational) motion about an axis parallel to the longitudinal axis of the wind tunnel was on occasion observed, especially at high flow speeds during the free-vibration tests. Correction of this problem, for example by restricting the rotational degree of freedom, was not possible with the current experimental setup. Any effect was again considered in the present context as part of the investigation on experimental variability.

Observing the variability of the coefficient of variation tends to confirm that the data are rather dispersed.

This trend seems clear in correspondence with the lowest and highest values of U_r , where it is believed that imperfect setup conditions may have also contributed to the results.

This conclusion was also noted in Figs. 5 and 6 at high reduced velocities. The range between 5 m/s and 10 m/s (U_r between 9 and 14, approximately) gives results less dependent on the reduced velocity, particularly for H_1^* , H_2^* , H_3^* and H_4^* (Figs. 7(a)-7(d)).

The standard deviation is almost constant in the range of velocities between about 3 m/s and 10 m/s (U_r between 6 and 14, approximately) for several of the derivatives; deviations start to appear in the proximity of the highest value of the reduced velocity.

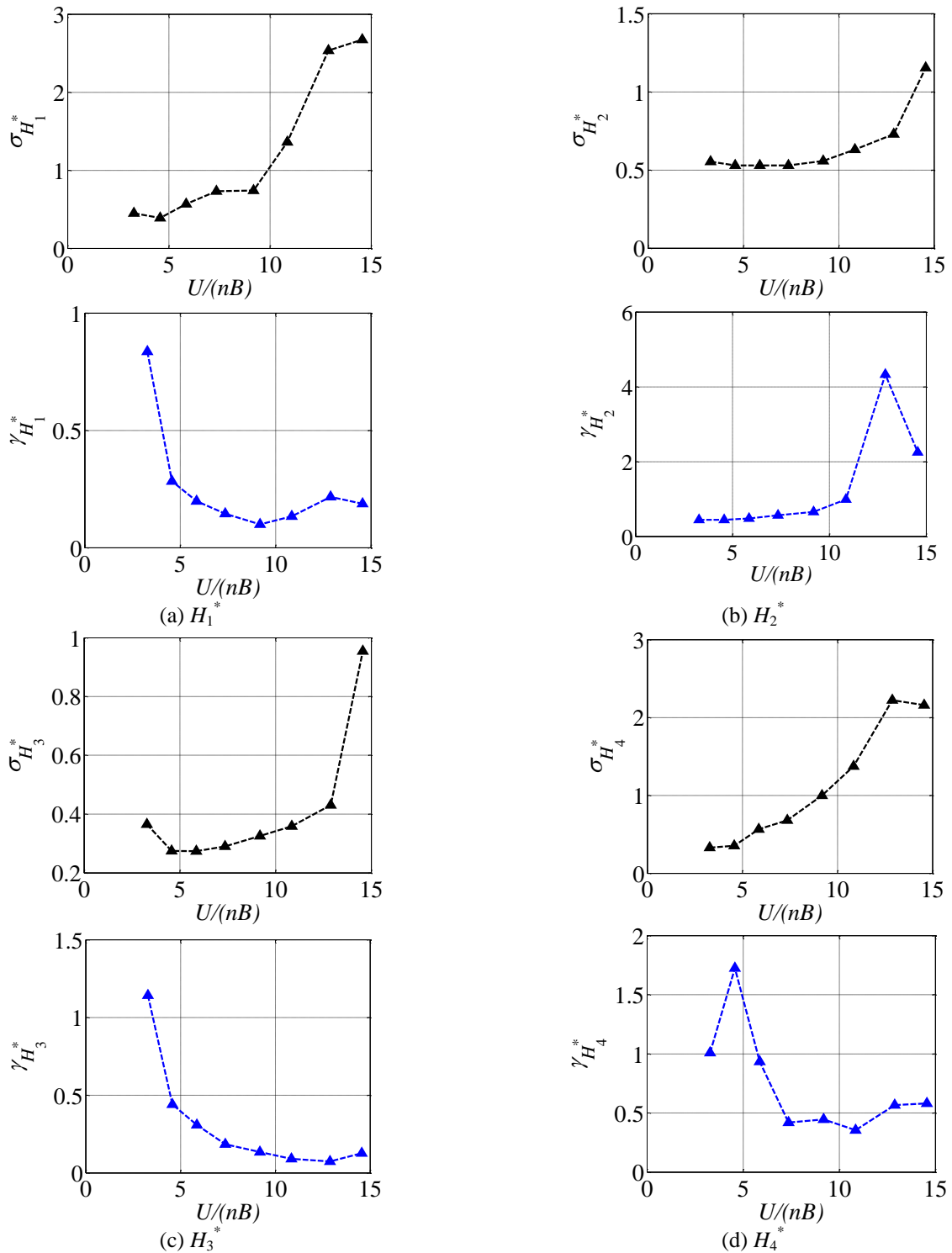


Fig. 7 Standard deviation and (σ) and coefficient of variation (γ) of the flutter derivatives (lift force)

Only the standard deviation of H_4^* and A_1^* , respectively reported in Figs. 7(d) and 8(a), does not exhibit the same trend common to other derivatives.

Generally, the coefficients of variation are high for the H_i^* flutter derivatives and smaller for the A_i^* ; in special cases, for example H_4^* and A_1^* , they appear to be greater than 1 for H_1^* , and for H_2^* they are larger than 0.5. This

additional examination of the data suggests that the mean graphs of the flutter derivatives cannot be used as representative values, for example in a flutter analysis. The importance of a more detailed analysis of the data is necessary before selecting “an appropriate value” of each flutter derivative for structural design.

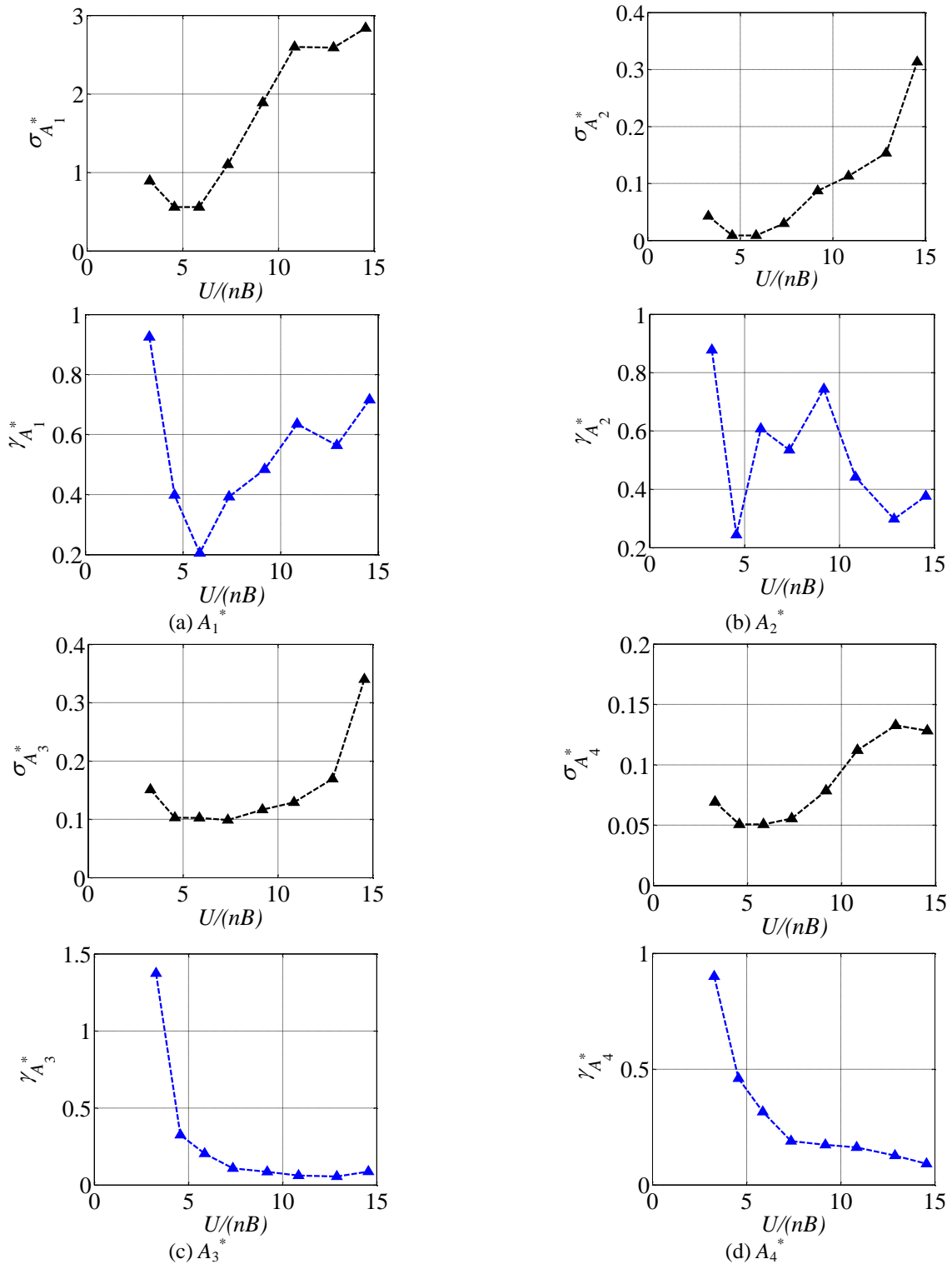
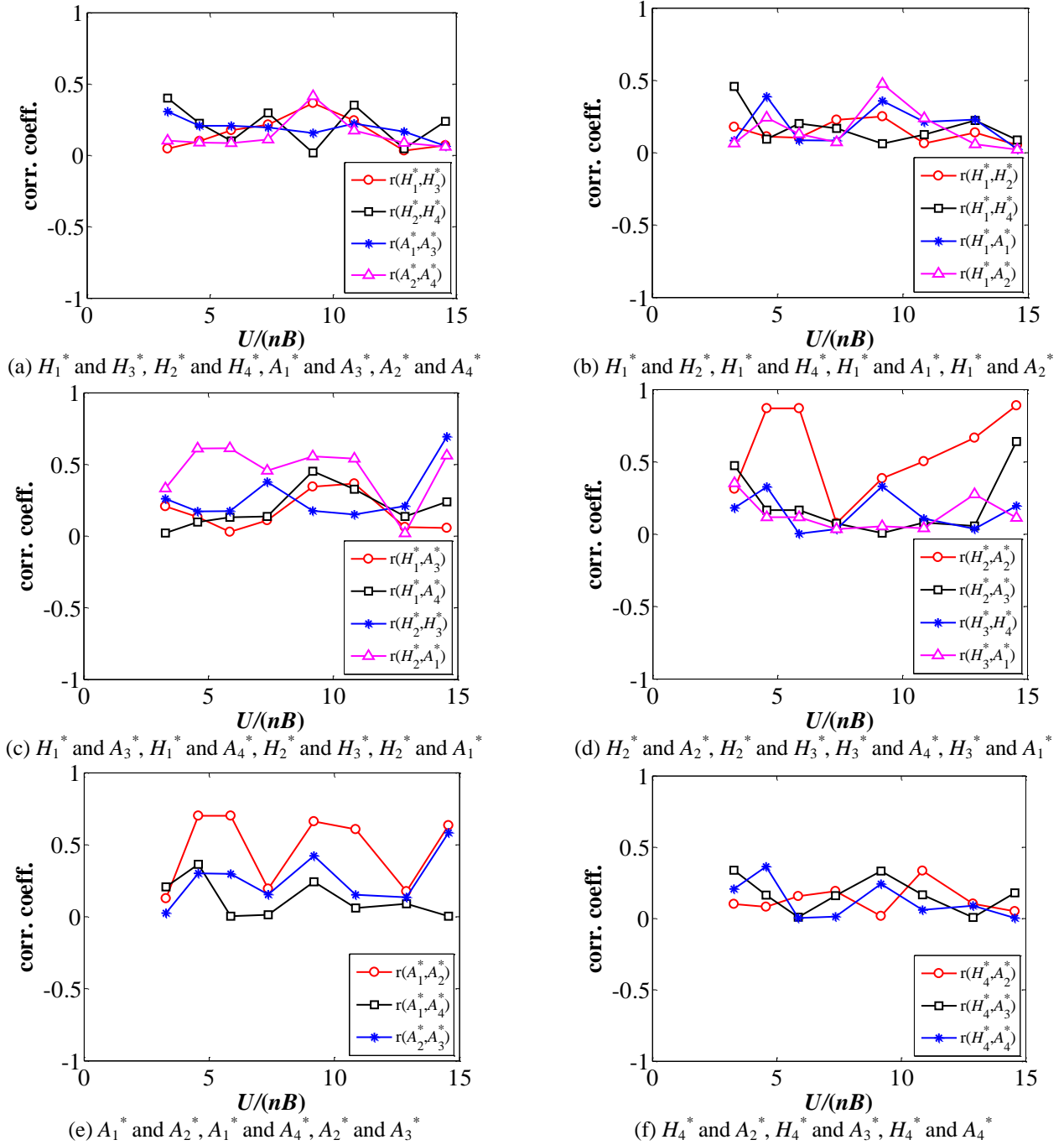


Fig. 8 Standard deviation and (σ) and coefficient of variation (γ) of the flutter derivatives (torsional moment)

5.2 Inter-dependency among flutter-derivative errors

In order to estimate the correlation between the different derivatives, the cross-correlation coefficients are also plotted for each couple of derivatives. In Fig. 9 examples of various combinations of cross-correlation coefficients are presented to investigate potential dependence. It may be

noted that inter-dependence among some flutter derivatives is possible: a relationship holds at large U_r between H_1^* and H_3^* , between A_1^* and A_3^* , between A_2^* and A_4^* (Scanlan *et al.* 1997), and between H_2^* and H_4^* (Matsumoto *et al.* 1996, Matsumoto and Abern 1998, Scanlan *et al.* 1997).

Fig. 9 Cross-correlation coefficient (r) of the flutter derivatives

It is therefore important to investigate the cross-correlation among the various acquisitions and to determine whether the variability is the result of experimental errors and imperfections in the setup or whether the theoretical results are influencing the correlations. The derivatives, which should (at least theoretically) exhibit correlation, are plotted in Fig. 9(a) as a function of the reduced velocity. The other combinations of the derivatives, which should not be correlated, are illustrated in Fig. 9(b) to Fig. 9(f).

Finally, in Table 4 the normalized variance-covariance matrix of a sub-set of the flutter derivatives is presented at selected reduced velocities.

The variance-covariance matrix is obtained according to Eq. (4) below, which is constructed using exclusively the terms H_1^* , H_3^* and A_2^* with the notation “cov” indicating the covariance mathematical operator

$$\underline{\Sigma} = \begin{bmatrix} \text{cov}(H_1^*, H_1^*) & \text{cov}(H_1^*, A_2^*) & \text{cov}(H_1^*, H_3^*) \\ \text{cov}(A_2^*, H_1^*) & \text{cov}(A_2^*, A_2^*) & \text{cov}(A_2^*, H_3^*) \\ \text{cov}(H_3^*, H_1^*) & \text{cov}(H_3^*, A_2^*) & \text{cov}(H_3^*, H_3^*) \end{bmatrix}. \quad (4)$$

Table 4 Normalized variance – covariance matrices at selected reduced velocities

$U_r=3.28$			$U_r=4.57$		
1.00	0.40	-0.56	1.00	0.40	-0.56
0.40	1.00	-0.98	0.40	1.00	-0.98
-0.56	-0.98	1.00	-0.56	-0.98	1.00
$U_r=5.86$			$U_r=7.36$		
1.00	-0.98	-0.07	1.00	0.48	0.11
-0.98	1.00	-0.22	0.48	1.00	0.92
-0.07	-0.22	1.00	0.11	0.92	1.00
$U_r=10.86$			$U_r=14.56$		
1.00	-0.97	0.51	1.00	-0.90	-0.47
-0.97	1.00	-0.70	-0.90	1.00	0.79
0.51	-0.70	1.00	-0.47	0.79	1.00

Referring to Eq. (4), the diagonal values are the variances of the individual flutter derivatives; the off-diagonal terms in the matrix are the co-variances between the specified two terms. In Table 4 the normalized elements are presented, i.e., normalized to obtain the correlation coefficients.

The study of the $\underline{\Sigma}$ matrix in Table 4 confirms the trend noted in Fig. 9(a). A small cross-correlation coefficient can be noted between H_1^* and H_3^* at all reduced velocities, on occasion less than 0.5; this remark seems to contradict the theoretical hypothesis of dependence between H_1^* and H_3^* . This result is perhaps unexpected. Nevertheless, it was interpreted that an imperfect correlation between derivatives, which are known to potentially be linked to one another (for example H_1^* and H_3^*), is still plausible because of random error; it could be associated with imperfect setup or variable test conditions that are responsible for the deviations from the reference values. It is also observed that these variations are possibly not linked to a physical phenomenon, i.e., a clear functional dependence between H_1^* and H_3^* , but are perhaps the result of a random test. Larger cross-correlation values are noted between H_1^* and A_2^* especially at high reduced velocities, although Fig. 9(b) indicates that it may, on occasion, become less than 0.5.

Consequently, the use of non-correlated random flutter derivatives may also be accepted, at least as a first approximation, in the context of experimental uncertainty propagation for the prediction of the bridge model response.

5.3 Experimental error quantification

In order to provide a measure of the data set variability and examine experimental and simulation errors, the confidence (CI) and tolerance (TI) intervals were also estimated. The reduced speed $U_r = 4.57$ is used as an example.

The confidence interval measures the deviation from the true value of the mean of a random variable (unknown) and the sample mean estimator. In the present study, it was approximately estimated as follows $CI_{(95\%)} \approx \bar{x}_\sigma \pm 1.96 \sigma / \sqrt{n_p}$, where 1.96 is the extent of a Gaussian distribution for a degree of confidence equal to 95% and n_p is the total number of sample realizations ($n_p = 30$ in this

example). This definition of $CI_{(95\%)}$ is exact if the error is normally distributed. Notoriously, the standard confidence interval equation relies on the population standard deviation. However, since the latter is not known, it is replaced in with the sample standard deviation. The estimated $CI_{(95\%)}$ is a fairly accurate approximation of the confidence interval for large samples (i.e., $n_p \geq 30$; Walpole *et al.* 2002).

The tolerance interval (TI) was estimated by the algebraic sum $\bar{x}_\sigma \pm k\sigma$ (for data sets with distribution approximately symmetric about \bar{x}_σ). The quantity k is the tolerance factor. In this study, k is defined such that there is a 99% confidence that the calculated tolerance limits will contain at least 95% of the measurements. If the Gaussian distribution is employed to approximate the data variability, $k=2.36$ may be used.

Fig. 10 presents examples of tolerance and confidence intervals of the experimental flutter derivatives, estimated by repeating experiments 30 times at each U_r . At $U_r = 4.57$, all data points are inside the TI, except for H_1^* for which the number of experimental data points located outside this interval is equal to one. The absolute error can be defined as $\varepsilon_{TI,A} \approx 2k\sigma$; it varies between 0.02 (for A_2^* , with mean value -0.03) and 1.32 (for A_1^* , with mean value 1.40) at $U_r=4.57$. The non-negligible variability in the flutter derivatives suggests that a modification of the experimental setup might be considered to decrease the TI and CI. However, results confirm the variability of the flutter derivatives that is reflected in the critical flutter speed estimation.

5.4 Supplementary analysis of the random variability in the flutter derivatives

The availability of repeated acquisitions (occurrences) of the various flutter derivatives suggested the possibility of conducting a more rigorous statistical analysis. In this subsection, an attempt was made to determine a set of suitable probability distributions, able to describe the variability observed in the wind tunnel experiments. To the authors' knowledge, few examples have been reported in the literature due to the limited systematic examination on uncertainty (e.g., Baldomir *et al.* 2013a, b). In previous studies by this research team (e.g., Seo and Caracoglia 2012) the probability distributions, used for flutter reliability, were in fact assumed *a priori* due to insufficient data sets along with several other simplifying assumptions.

This study was carried out by examining all flutter derivatives, H_i^* and A_i^* with $i=1, \dots, 4$ at all reduced velocities. In the following, results for H_i^* and A_i^* with $i=1, \dots, 3$ at four distinct U_r values equal to 4.57, 7.36, 10.86 and 14.56 are shown.

In each investigation the flutter derivative data, 30 repetitions and acquisitions at each pre-selected U_r , were initially normalized as $H_i^*/H_{i,m}^*$ and $A_i^*/A_{i,m}^*$, in which $H_{i,m}^*$ and $A_{i,m}^*$ are the mean values at the corresponding U_r (also visible in Figs. 5 and 6). This normalization was preferred to eliminate the dependence on the sign of the derivative, which enables the subsequent comparison of the empirical probability distributions with several models of random variables.

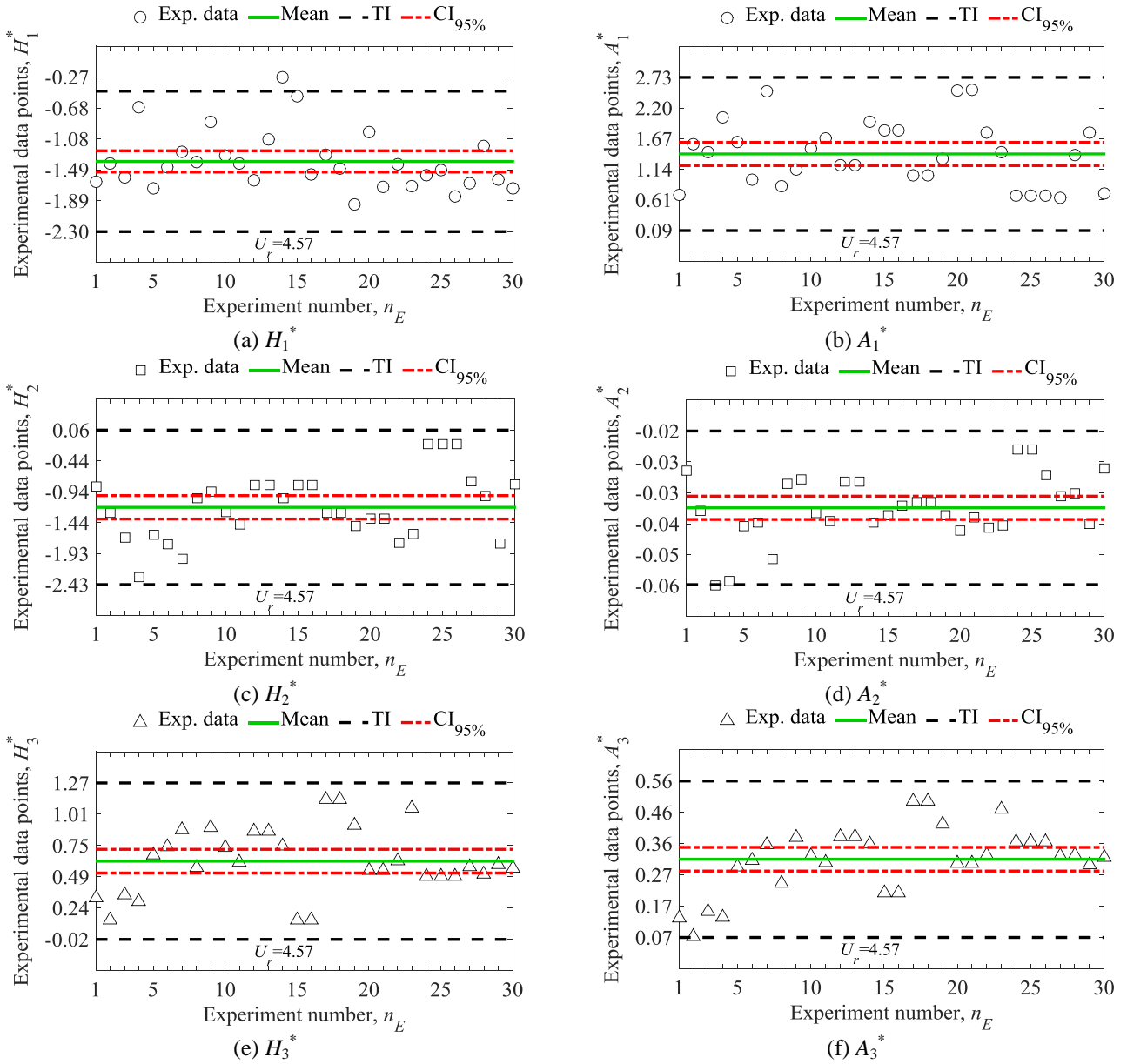


Fig. 10 Analysis of experimental datasets, tolerance (TI) and confidence intervals (CI) of several derivatives at reduced velocity $U_r=4.57$

These models include the following distributions: Gaussian, Log-normal, Gamma and Weibull. It must be noted that the selection of the models was dictated in part by findings discussed in previous studies (Seo and Caracoglia 2012, Caracoglia 2013, Canor *et al.* 2015).

The results of this investigation are presented in Fig. 11 for $H_1^*/H_{1,m}^*$ and $H_{1,3}^*/H_{1,3,m}^*$, and in Fig. 12 for $A_1^*/A_{1,m}^*$ and $A_2^*/A_{2,m}^*$.

In each panel of the two figures the empirical cumulative distribution function (CDF), derived from each data set by “plotting position” (each data point indicated by a black marker), is plotted against the CDF functions corresponding to the four selected models. The parameters of each probability model were determined by maximum likelihood estimation using the actual data.

From the various panels of the two figures it can be observed that each of the distribution models is capable of partially replicating the trends in the data. The probability distributions are not the same at various U_r ; this remark is confirmed by the observations on the variable standard deviation in the previous sections. In general, the four selected probability models more closely follow the experimental data at larger U_r .

A less accurate behavior is evident close to the tails of the distributions (for example the lower tail in $H_1^*/H_{1,m}^*$ at $U_r=4.57$ in Fig. 11(a)). On occasion, this trend is noted toward the median values of the CDF (Fig. 11(a) for $H_1^*/H_{1,m}^*$ at $U_r=4.57$) or the upper tails or quantiles (Fig. 12(b) for $A_2^*/A_{2,m}^*$ at $U_r=4.57$).

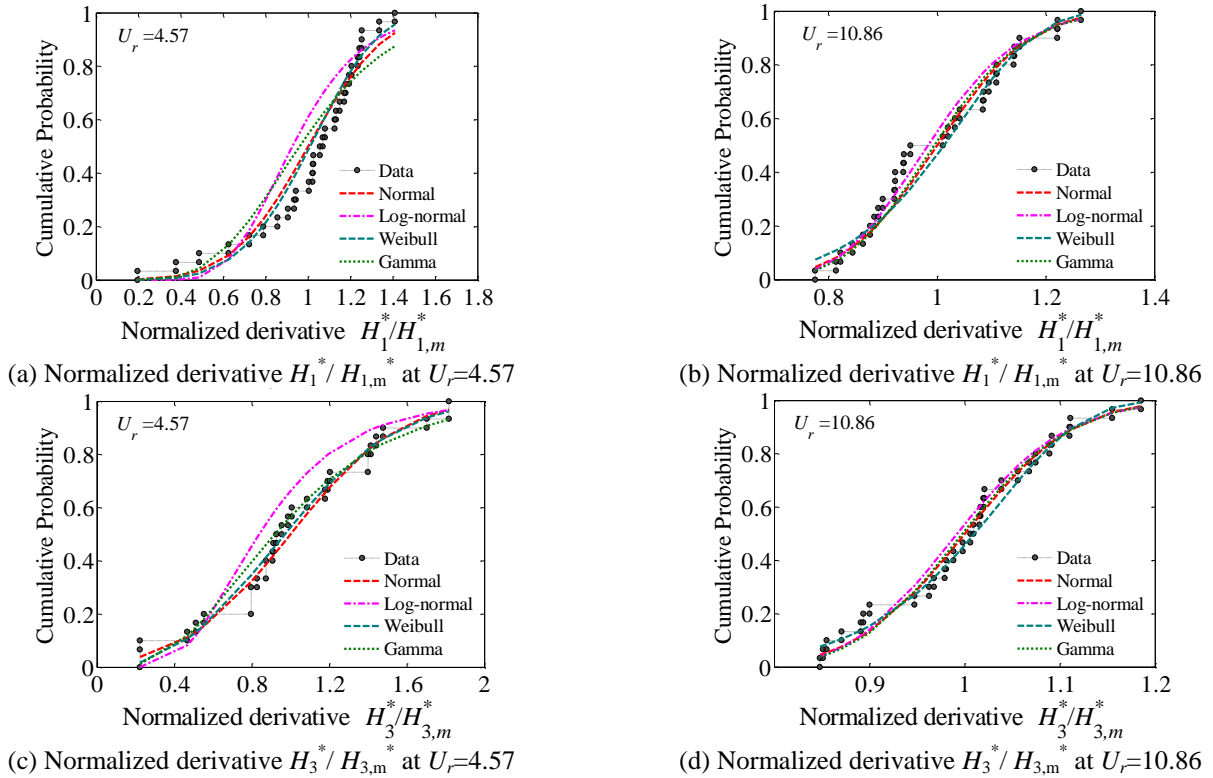


Fig. 11 Cumulative distribution function (CDF) of the lift-related derivatives

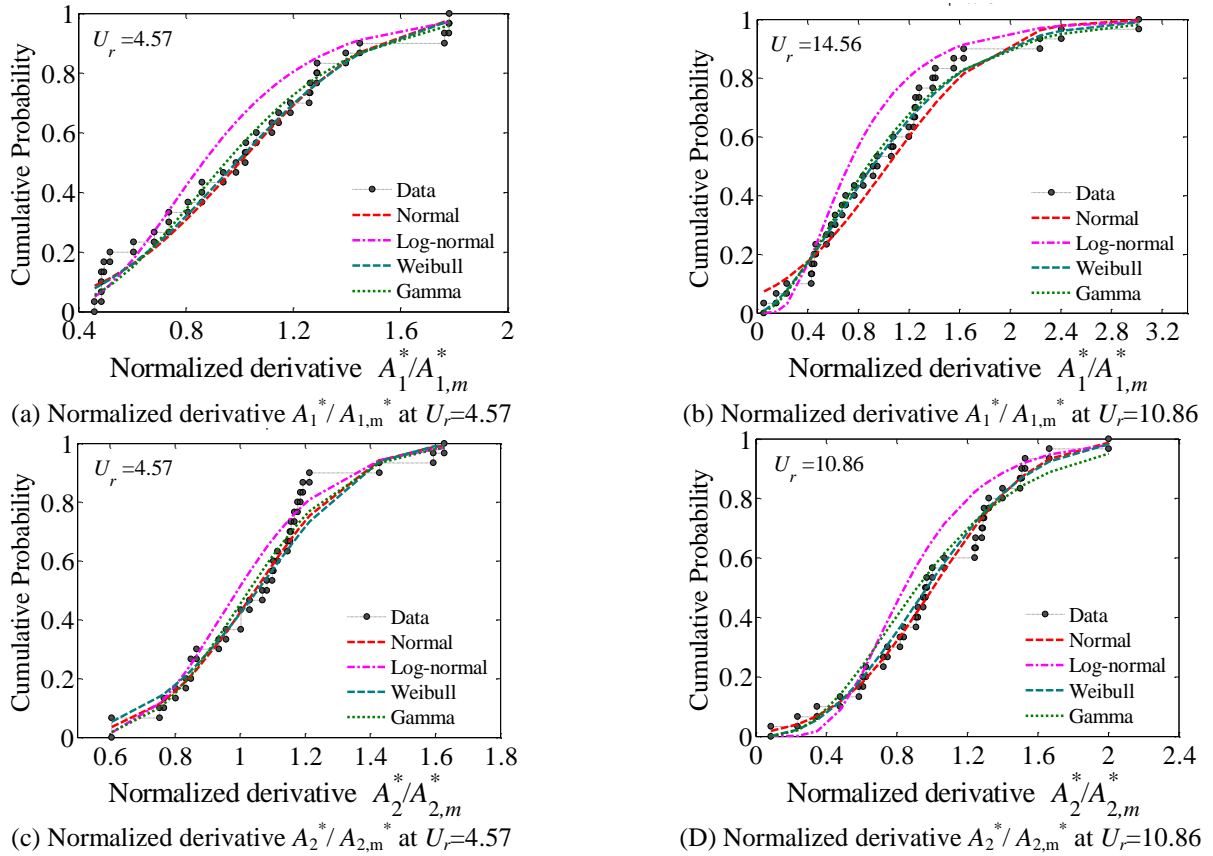


Fig. 12 Cumulative distribution function (CDF) of the moment-related derivatives

A quantitative examination of the various probability models was also carried out by means of hypothesis testing, applied to all cases presented in Figs. 11 and 12. The one-sample Kolmogorov-Smirnov (KS) test was employed to test the null hypothesis that the sample population was indeed derived from each of the four selected models. The main findings of the hypothesis testing are only presented, whereas the specific results of the analysis are not reported for the sake of brevity.

For example, the examination of the p -values corresponding to the Kolmogorov-Smirnov test for $H_{1,m}^*/H_{1,m}^*$, indicated that representation of the variability through both Log-normal and Gamma distributions is dubious at the significance level of 0.20 (especially at $U_r=4.57$), thereby excluding these two candidates. In contrast, the test does not seem to provide indication on either Gaussian or Weibull distribution. Physically, a Gaussian distribution is representative of a random measurement error with equally probable positive/negative deviations from the mean value. On the contrary, a Weibull model has a non-symmetrical distribution, potentially related to a physical explanation, for example the fact that a random flutter derivative does not likely change its sign at a given value of U_r . Visual inspection of Fig. 11(a) tends to confirm these observations, for example suggesting that the Gaussian model could approximately fit the data points. Moreover, it might possibly be more applicable to simulate the effect of a random measurement error.

In the case of $A_{2,m}^*/A_{2,m}^*$, which is another important derivative for the study of the aeroelastic behavior, the same observation was not found after null hypothesis testing. Exclusion of the candidates or selection of a unique probability distribution model appeared more difficult. For example, the four CDF functions are substantially overlapping at $U_r=4.57$ in Fig. 12(b). Besides, the Gaussian and Weibull distributions are practically coincident in Fig. 12(d).

5.5 Generalized representation of the random variability in the flutter derivatives by polynomial chaos expansion

Despite indications provided in the previous sub-section, none of the probability models could consistently replicate the observations across all U_r . Therefore, a supplementary investigation was carried out. A more generalized model of a random variable was used to explain the collected data. The spectral representation of a random variable or polynomial chaos expansion (Ghanem and Spanos 1991) was employed. This approach is briefly introduced in this section.

On a probability space (Θ, Σ, P) , if one denotes by θ the random event belonging to the domain Θ , a generic realization of a random variable, for example H_i^* and A_i^* at a given U_r , can be formally written as $H_i^*(U_r; \theta)$ and $A_i^*(U_r; \theta)$. The representation of the random H_i^* and A_i^* derivatives can be expressed as, with $i=1, \dots, 4$:

$$H_i^*(U_r; \theta) = \sum_{j=0}^P h_{i,j}^* \psi_j(\xi(\theta)) \quad (5a)$$

$$A_i^*(U_r; \theta) = \sum_{j=0}^P a_{i,j}^* \psi_j(\xi(\theta)) \quad (5b)$$

In the previous equations, the truncation order of the expansion is denoted by P ; the quantities ψ_j are polynomials of degree j used by the expansion; $\xi(\theta)$ is a realization of a “seed” random variable; the quantities $h_{i,j}^*$ and $a_{i,j}^*$ are normalized scalar coefficients of the polynomial chaos expansion that need to be determined. This representation basically transforms a “seed” random variable $\xi(\theta)$ into a “more general” random variable by nonlinear translation process (Grigoriu 2002). The polynomials ψ_j are selected as mutually orthogonal with respect to the probability density function of the seed variable. The seed is usually represented by a standard Gaussian variable recast in terms of normalized Hermite polynomials ψ_j (or “Hermite chaos”), as in the original polynomial chaos decomposition (Ghanem and Spanos 1991). More recently, Askey-Wilson polynomials were shown to be useful and employed to describe even more general distributions (Xiu and Karniadakis 2002).

The representation in Eq. (5) has been successfully applied to the representation of the probabilities of several random variables (scalar or vectors) obtained from experimental data. Some examples are elastic properties of random media (Desceliers *et al.* 2007) and uncertain stiffness properties of instrumented structures (Schoefs *et al.* 2011). In wind engineering, this representation and the concept of translation process based on the “Hermite model” were efficaciously employed to replicate non-Gaussian features of intermittent wind pressure fields (Gurley and Kareem 1997) and the non-Gaussian extreme values of the response in wind-excited structures (Ding and Chen 2014). Recently, the polynomial chaos expansion and the corresponding spectral methods were explored to study flutter probability, contaminated by errors in flutter derivatives (Canor *et al.* 2015).

The polynomial chaos expansion requires the coefficients $h_{i,j}^*$ and $a_{i,j}^*$ to be estimated. In this study, the numerical procedure proposed by Schoefs *et al.* (2011) was utilized to determine $h_{i,j}^*$ and $a_{i,j}^*$.

These coefficients were found from the minimization of the negative log-likelihood function evaluated at the experimental points (30 acquisitions of the flutter derivative at each pre-selected value of U_r), using as PDF the function corresponding to the Hermite chaos at a given P -th degree of the polynomials.

The procedure for finding $h_{i,j}^*$ and $a_{i,j}^*$ coincides with a minimization problem that is solved by scansion of the parameter space. As first observed by Desceliers *et al.* (2007) this optimization must follow certain constraints. For example, since $\psi_0(\xi) = 1$ in the Hermite chaos, $h_{1,0}^*$ and $a_{1,0}^*$ are simply the mean values of the sample (denoted as $H_{i,m}^*$ and $A_{i,m}^*$ at a given U_r in the previous sub-section).

Moreover, Desceliers *et al.* (2007) show that the normalized variance of the sample must be equal to the relationship $\sum_{j=1}^P (h_{i,j}^*)^2$ and $\sum_{j=1}^P (a_{i,j}^*)^2$. Description of

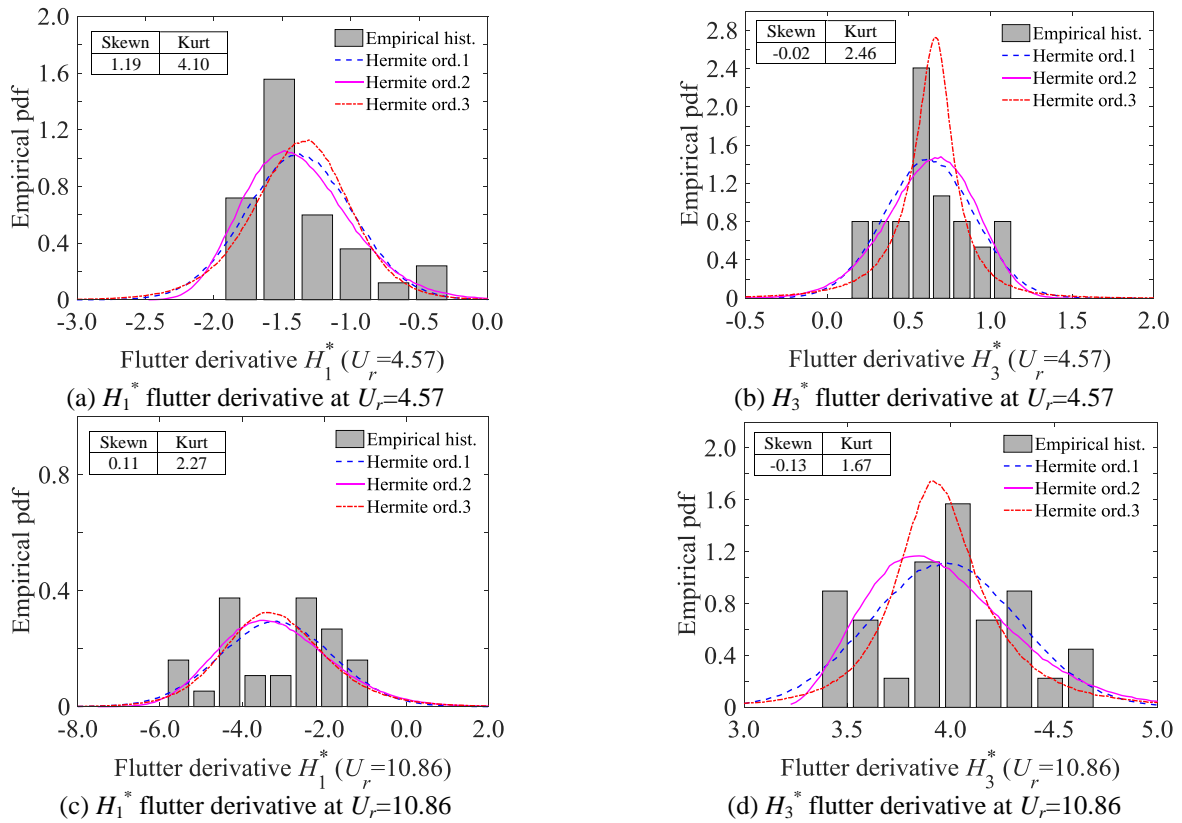


Fig. 13 Probability density function (PDF) of H_1^* and H_3^* flutter derivatives

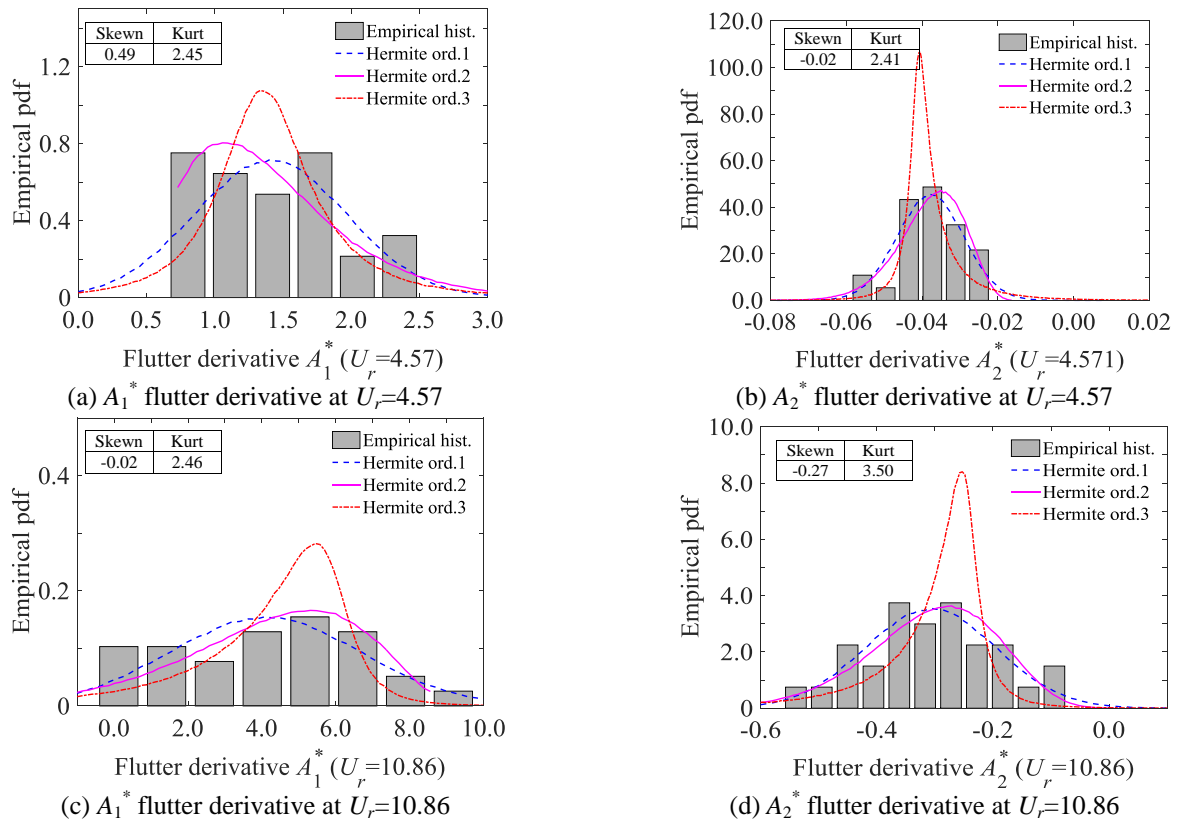


Fig. 14 Probability density function (PDF) of A_1^* and A_2^* flutter derivatives

the numerical procedure, employed herein, is omitted for the sake of brevity but may be found in Schoefs *et al.* (2011).

Various types of Hermite chaos [order of the expansions P in Eqs. (5)] were considered to identify non-linear and non-Gaussian features and to verify the observations in Section 5.4. The investigation was restricted to the “most important” derivatives, H_1^* and H_3^* , and A_1^* and A_2^* at four representative reduced velocities. Contrary to the previous sub-section, no normalization of the experimental data was used prior to the estimation of polynomial chaos coefficients.

Figs. 13 and 14 present the results. The graphs compare the empirical PDF functions (thirty repeated acquisitions) with the PDF curves found by applying the procedure described above and Eq. (5). The empirical histogram of occurrences (empirical PDF) is compared against various probability functions determined through Hermite-chaos polynomial expansion of various orders.

Figs. 13 and 14 also report the skewness (“Skewn”) and kurtosis (“Kurt”) determined from the experimental sample. The skewness ranges from -0.27 (i.e. for A_2^* with $U_r=10.86$, Fig. 14d) to 1.19 (i.e., for H_1^* with $U_r=4.57$, Fig. 13(a)); the kurtosis is between 1.68 (i.e., for H_3^* with $U_r=10.86$, Fig. 13(d)) and 4.10 (i.e., for H_1^* with $U_r=4.57$, Fig. 13(a)). In all cases it can be noted that the empirical PDFs (histograms) are sharper than the Gaussian distribution, corresponding to a Hermite model with order $P=1$ in the figures (“Hermite ord. 1”), and that long tails are possible (for example for H_1^*). For all derivatives and reduced velocities, the first-order expansion (i.e., a Gaussian distribution) appears to be unsuitable since is not capable of replicating some features of the empirical data sets. Higher order chaos expansion was more adequate. Similar observations were approximately found for other derivatives and other values of the reduced velocity.

6. Examining flutter speed of the 2DOF setup, accounting for experimental variability

As previously described, the evaluation of the critical flutter speed can be carried out by independently examining each realization (or identification) of the experiments, i.e., by using a combination of thin light-colored lines in Figs. 5 and 6 instead of the mean graphs. This operation can be repeated 30 times by assuming independence among the experiments at various U . For each set of derivatives, the critical flutter speed of the wind-tunnel section model was found in accordance with the procedure by Simiu and Scanlan (1986) and previously outlined (Section 4.3). Each solution represents one possible critical flutter solution contaminated by measurement variability.

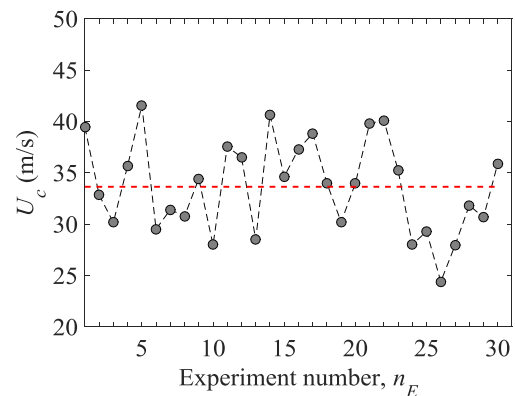
The results of this examination are presented in Figs. 15(a) and 15(b). Each solution, experiment by experiment, was converted to critical flutter speed (U_c) and critical angular flutter frequency (ω_c). In Fig. 15(a) the sample mean of U_c is reported using a dashed line; the mean value is equal to 32.50 m/s, whereas the median is equal to 33.98 m/s. The critical speed U_c of the wind-tunnel section model

(Fig. 15(a)) varies (stochastically) between about 24.4 m/s and 41.5 m/s. Relative variations with respect to the mean value are, respectively, between -20% and +20% (i.e., the standard deviation is equal to 4.53). Results indicate non-negligible variability in a range of wind speeds larger than the one examined experimentally and compatible with the observations.

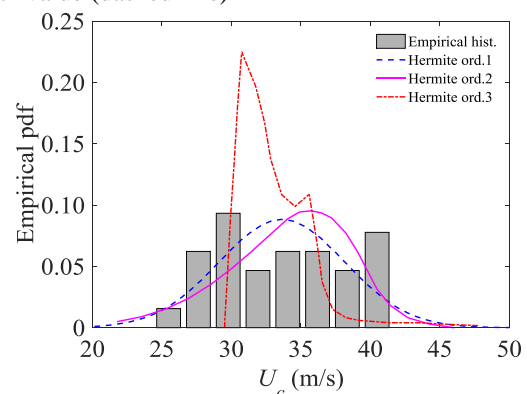
Results also suggest that variability in the flutter threshold of this section model may not be insignificant and confirms the need for probabilistic analysis of the flutter condition, accounting for experimental aeroelastic-load variability.

According to the method described in Section 5.5, Hermite polynomials of various orders using the standard Gaussian “seed” can also be used to enable the stochastic analysis of the sample of U_c (thirty experimental values).

Fig. 15(b) illustrates the results of the stochastic analyses. The figure shows a comparison between the empirical PDF of the critical speed U_c evaluated from the histogram of the data, and the PDF estimated by Hermite chaos using the procedure described in Section 5.5. The empirical PDF of the critical speed U_c exhibits a positive skewness whereas; the 1st order of polynomial chaos results in a shifted normal distribution (as expected); the 2nd order expansion results in a negative skewness. Finally, the PDF obtained with a 3rd-order Hermite polynomial has a positive skewness; it shows a peak around 30 m/s, close to the empirical histogram of U_c .



(a) Variation of critical flutter speed U_c compared to its mean value (dashed line)



(b) Probability density function (PDF) of U_c

Fig. 15 Critical flutter speed U_c calculated using 30 sets of flutter derivatives, measured in wind tunnel

Nevertheless, the behavior in the tails of the distribution is dissimilar from the empirical data of U_c . These discrepancies are possibly attributed to the limited number of experimental realizations, which were used to determine the Hermite expansion coefficients of the U_c model, and possibly affected by the numerical solution of the flutter equation. The sample size (30) is small in comparison with literature recommendations (e.g., Schoefs *et al.* 2011); this limitation was unfortunately controlled by the number of experiments. Even though the polynomial chaos expansion suggested promising results for representation of flutter derivatives (Section 5.5), the same remark cannot be made for the critical speed. Using a different set of polynomials may be needed (Xiu and Karniadakis 2002). This additional study is beyond the scope of this paper and may possibly be considered in the future.

7. Conclusions

The purpose of this paper was to examine the variability of the Scanlan (flutter) derivatives, evaluated in wind tunnel, for a typical section model of a closed-box bridge girder. This objective was achieved by investigating the statistical properties and the probability distributions of the experimentally-determined flutter derivatives at various reduced velocities. Properties included: standard deviations, cross-correlation coefficients, variance-covariance matrix. Analysis was also expanded to identify a suitable model for describing the probability distribution of the derivatives. Significant experimental data variability was found. Consequently, using the mean value of the flutter derivatives, is not a representative quantity that can be used for bridge design. Error analysis is therefore desirable to verify variability in the structural bridge response.

Results also indicated a non-negligible variability in the flutter critical speed of the wind-tunnel section model, in a range variable between about 25 and 40 m/s.

The Gaussian distribution may be used, as a first approximation only, to describe variability in the flutter derivatives. No distribution model appears to suitably describe experimental variability at all reduced velocities and, consequent variability in the flutter speed of the section model. The study suggests that non-parametric methods, such as the polynomial chaos expansion, are very helpful and can be used to more accurately represent the data variability, to replicate skewness and long tails in the empirical distributions of both flutter derivatives and flutter speed.

In any case, the present study is an initial investigation; further studies are necessary to confirm the results for other deck geometries and laboratory conditions. Observed experimental variability is also associated with the specific experimental setup and unavoidable laboratory constraints. A better design of the “release system” and experimental setup might have further reduced variability in the initial conditions of the free-decay tests and, consequently, partially eliminated the experimental variability. An enhanced setup design should possibly be considered in the future.

Acknowledgments

Professor Piero D’Asdia, University of Chieti-Pescara “G. D’Annunzio”, Italy, is gratefully acknowledged for providing the initial motivation for this project and for his guidance during the preparation of the manuscript. Professor Oreste S. Bursi, University of Trento, Italy, is gratefully acknowledged for valuable discussion on uncertainty propagation and polynomial chaos expansion during the sabbatical leave of Luca Caracoglia in 2014 and 2015.

Messrs. Kurt Braun and Michael MacNeil of NEU’s Department of Civil and Environmental Engineering are gratefully acknowledged for construction and assembly of the experimental setup and for technical assistance during the execution of the tests. The authors would also like to thank Messrs. David Abati and Darren Vokes of NEU’s Carpentry Department for the fabrication of the section models and for the design and assembly of the test chamber. Professor Jerome F. Hajjar and the NEU’s Department of Civil and Environmental Engineering are gratefully acknowledged for the collaboration with sensor equipment. Finally, the authors would like to thank the NEU’s Department of Mechanical and Industrial Engineering for the shared use of wind tunnel facility.

References

- Argentini, T., Pagani, A., Rocchi, D. and Zasso, A. (2014), “Monte Carlo analysis of total damping and flutter speed of a long span bridge: Effects of structural and aerodynamic uncertainties”, *J. Wind Eng. Ind. Aerod.*, **128**, 90-104.
- Baldomir, A., Hernández, S., Nieto, F. and Jurado, J. (2013a), “Reliability analysis of flutter speed in long span bridges using FORM technique”, *Proceedings of the 13th International Conference on Wind Engineering (ICWE 13)*, Amsterdam, NL.
- Baldomir, A., Kusano, I., Jurado, J.A. and Hernández, S. (2013b), “A reliability study for the Messina Bridge with respect to flutter phenomena considering uncertainties in experimental and numerical data”, *Comput. Struct.*, **128**, 91-100.
- Bartoli, G., Borri, C. and Gusella, V. (1997), “On the influence of wind turbulence on bridge deck flutter”, (Eds., Meskouris, K. Vittek, U.), *Aspects in modern computational structural analysis*. Balkema, Rotterdam, NL, 3-17.
- Bendat, J.S. and Piersol, A.G. (2000), *Random Data Analysis and Measurement Procedures*, 3rd Ed., John Wiley and Sons, New York, NY, USA.
- Brito, R. and Caracoglia, L. (2009), “Extraction of flutter derivatives from small scale wind tunnel experiments”, *Proceedings of the 11th Americas Conference on Wind Engineering*, American Association for Wind Engineering (AAWE), San Juan, Puerto Rico, June 22-26, 2009, CD-ROM.
- Bucher, C.G. and Lin, Y.K. (1988), “Stochastic stability of bridges considering coupled modes”, *J. Eng. Mech. - ASCE*, **114**(12), 2055-2071.
- Canor, T., Caracoglia, L. and Denoël, V. (2015), “Application of random eigenvalue analysis to assess bridge flutter probability”, *J. Wind Eng. Ind. Aerod.*, **140**, 79-86.
- Caracoglia, L. (2013), “An Euler–Monte Carlo algorithm assessing Moment Lyapunov Exponents for stochastic bridge flutter predictions”, *Comput. Struct.*, **122**, 65-77.
- Chen, A., He, X. and Xiang, H., (2002), “Identification of 18 flutter derivatives of bridge decks”, *J. Wind Eng. Ind. Aerod.*,

- 90(12-15), 2007-2022.
- Chen, A., Xu, F. and Ma, R. (2006), "Identification of flutter derivatives of bridge decks using stochastic search technique", *Wind Struct.*, **9**(6), 441-455.
- Cheng, J., Cai, C.S., Xiao, R.C. and Chen, S.R. (2005), "Flutter reliability analysis of suspension bridges", *J. Wind Eng. Ind. Aerod.*, **93**(10), 757-775.
- Chowdhury, A.G. and Sarkar, P.P. (2003), "A new technique for identification of eighteen flutter derivatives using a three-degree-of-freedom section model", *Eng. Struct.*, **25**(12), 1763-1772.
- Chowdhury, A.G. and Sarkar P.P. (2004), "Identification of eighteen flutter derivatives of an airfoil and a bridge deck", *Wind Struct.*, **7**(3), 187-202.
- Desceliers, C., Soize, C. and Ghanem, R. (2007), "Identification of chaos representations of elastic properties of random media using experimental vibration tests", *Comput. Mech.*, **39**(6), 831-838.
- Ding, J. and Chen, X. (2014), "Assessment of methods for extreme value analysis of non-Gaussian wind effects with short-term time history samples", *Eng. Struct.*, **80**, 75-88.
- Dragomirescu, E., Miyata, T., Yamada, H. and Katsuchi, H. (2003), "Probabilistic approach of structural reliability applied to bridge components", *Proceedings of the 11th International Conference on Wind Engineering (11-ICWE)*, Texas Tech University, Lubbock, Texas, USA, Vol. 1, 789-796.
- Ge, Y.J., Xiang, H.F. and Tanaka, H. (2000), "Application of a reliability analysis model to bridge flutter under extreme winds", *J. Wind Eng. Ind. Aerod.*, **86**(2-3), 155-167.
- Ghanem, R. and Spanos, P.D. (1991), *Stochastic Finite Elements: A Spectral Approach*, Springer-Verlag, New York, New York, USA.
- Grigoriu, M. (2002), *Stochastic calculus. Applications in science and engineering*, Birkhäuser, Boston, MA, USA.
- Gu, M., Zhang, R. and Xiang H. (2001), "Parametric study on flutter derivatives of bridge decks", *Eng. Struct.*, **23**(12), 1607-1613.
- Gurley, K. and Kareem, A. (1997), "Analysis, interpretation, modeling and simulation of unsteady wind and pressure data", *J. Wind Eng. Ind. Aerod.*, **69-71**, 657-669.
- Hračov, S., Náprstek, J. and Pospíšil, S. (2005), "Flutter stability condition of bluff body with respect to stochastic approach". *Proceedings of the 10th Americas Conference on Wind Engineering (10ACWE)*, Baton Rouge, Louisiana, USA, CD-ROM.
- Huston, D.R., Bosch, H.R. and Scanlan, R.H. (1988), "The effects of fairings and of turbulence on the flutter derivatives of a notably unstable bridge deck". *J. Wind Eng. Ind. Aerod.*, **29**(1-3), 339-349.
- Jain, A. (1996), "Multi-mode aeroelastic and aerodynamic analysis of long-span bridges", PhD Dissertation, Johns Hopkins University, Baltimore, Maryland, USA.
- Jain, A., Jones, N.P. and Scanlan, R.H. (1996), "Coupled aeroelastic and aerodynamic response analysis of long-span bridges", *J. Wind Eng. Ind. Aerod.*, **60**(1-3), 69-80.
- Jerri, A.J. (1977), "The Shannon sampling theorem-its various extensions and applications: a tutorial review", *Proceedings of the IEEE*, **65**(11), 1565-1596.
- Jones, N.P. and Scanlan, R.H. (2001), "Theory and full-bridge modeling of wind response of cable-supported bridges", *J. Bridge Eng. - ASCE*, **6**(6), 365-375.
- Katsuchi, H., Jones, N.P. and Scanlan, R.H. (1999), "Multimode coupled buffeting and flutter analysis of the Akashi-Kaikyo Bridge", *J. Struct. Eng. - ASCE*, **125**(1), 60-70.
- Khalil, M., Poirel, D. and Sarkar, A. (2016), "Bayesian analysis of the flutter margin method in aeroelasticity", *J. Sound Vib.*, **384**, 56-74.
- Kim, H.-K., Shinozuka, M. and Chang, S.-P. (2004), "Geometrically nonlinear buffeting response of a cable-stayed bridge", *J. Eng. Mech. - ASCE*, **130**(7), 848-857.
- Kwon, S.D. (2010), "Uncertainty of bridge flutter velocity measured at wind tunnel tests", *Proceedings of the 5th International Symposium on Computational Wind Engineering (CWE2010)*, Chapel Hill, North Carolina, USA, May 23-27, 2010, CD-ROM.
- Lin, Y.K. and Ariaratnam, S.T. (1980), "Stability of bridge motion in turbulent winds", *J. Struct. Mech.*, **8**(1), 1-15.
- Mannini, C. and Bartoli, G. (2007), "A probabilistic approach to bridge deck flutter", *Proceedings of the 12th International Conference on Wind Engineering (ICWE12)*, Cairns, Australia, 2351-2358.
- Matsumoto, M. (1996), "Aerodynamic damping of prisms", *J. Wind Eng. Ind. Aerod.*, **59**(2-3), 159-175.
- Matsumoto, M. and Abern, K. (1998), "Role of coupled derivatives on flutter instabilities", *Wind Struct.*, **1**(2), 175-181.
- Matsumoto, M., Kobayashi, Y. and Shirato, H. (1996), "The influence of aerodynamic derivatives on flutter", *J. Wind Eng. Ind. Aerod.*, **60**, 227-239.
- Náprstek, J. and Pospíšil, S. (2004), "Flutter onset influenced by combined multiplicative and additive random noises". *Proceedings of the 5th International Colloquium on Bluff Body Aerodynamics and Applications (BBAA V)*, Ottawa, Ontario, Canada, 289-292.
- Pospíšil, S., Náprstek, J. and Hračov, S. (2006), "Stability domains in flow-structure interaction and influence of random noises", *J. Wind Eng. Ind. Aerod.*, **94**(11), 883-893.
- Pourzeynali, S. and Datta, T.K. (2002), "Reliability analysis of suspension bridges against flutter", *J. Sound Vib.*, **254**(1), 143-162.
- Qin, X. and Gu, M. (2004), "Determination of flutter derivatives by stochastic subspace identification technique", *Wind Struct.*, **7**(3), 173-186.
- Sarkar, P.P. (1992), "New identification methods applied to the response of flexible bridges to wind", PhD Dissertation, Johns Hopkins University, Baltimore, MD, USA.
- Sarkar P.P., Caracoglia L., Haan, F.L., Sato, H. and Murakoshi, J. (2009), "Comparative and sensitivity study of flutter derivatives of selected bridge deck sections. Part 1: Analysis of inter-laboratory experimental data", *Eng. Struct.*, **31**(1), 158-169.
- Sato, H., Murakoshi, J. and Fumoto, K. (2004), "Benchmark Study on flutter derivatives - Measurements at PWRI, Japan", Unpublished Research Report, Structures Research Group, Public Works Research Institute, Tsukuba, Japan.
- Scanlan, R.H. and Jones, N.P. (1990), "Aeroelastic analysis of cable-stayed bridges", *J. Struct. Eng. - ASCE*, **116**(2), 279-297.
- Scanlan, R.H., Jones, N.P. and Singh, L. (1997), "Inter-relations among flutter derivatives", *J. Wind Eng. Ind. Aerod.*, **69-71**, 829-837.
- Scanlan, R.H. and Tomko, J.J. (1971), "Airfoil and bridge deck flutter derivatives", *J. Eng. Mech. - ASCE*, **97**(6), 1717-1737.
- Schoefs, F., Yáñez-Godoy, H. and Lanata, F. (2011), "Polynomial chaos representation for identification of mechanical characteristics of instrumented structures", *Comput.-Aided Civil Infrastruct. E.*, **26**(3), 173-189.
- Seo, D.W. and Caracoglia, L. (2012), "Statistical buffeting response of flexible bridges influenced by errors in aeroelastic loading estimation", *J. Wind Eng. Ind. Aerod.*, **104-106**, 129-140.
- Sepe, V. and D'Asdia, P. (2003), "Influence of low-frequency wind speed fluctuations on the aeroelastic stability of suspension bridges", *J. Wind Eng. Ind. Aerod.*, **91**(10), 1285-1297.
- Sepe V. and Vasta M. (2014), "Aeroelastic stability of long span bridges: comparison between quasi-deterministic and POD-based representation of the wind turbulence". In: Cunha, A.,

- Caetano, E., Ribeiro, P., Müller, G.,(Eds.), *Proceedings of the 9th International Conference on Structural Dynamics*, (EURODYN 2014), 2855–2860, ISSN: 2311-9020, ISBN: 978-972-752-165-4.
- Sharan, S., M., Krishen, K. and Prem, K. (2008), “Relevance of eighteen flutter derivatives in wind response of a long-span cable-stayed bridge”, *J. Struct. Eng.*, **134**(5), 769-781.
- Simiu, E. and Scanlan, R.H. (1986), *Wind Effects on Structures*, 2nd edition, John Wiley & Sons, New York, N.Y., USA.
- Starossek, U., Aslan, H. and Thiesemann, L. (2009), “Experimental and numerical identification of flutter derivatives for nine bridge deck sections”, *Wind Struct.*, **12**(6), 519-540.
- Tsiatas, G. and Sarkar, P.P. (1988), “Motion stability of long-span bridges under gusty winds”, *J. Eng. Mech. - ASCE*, **114**(2), 257-276.
- Xiu, D. and Karniadakis, G.E. (2002), “The Wiener-Askey polynomial chaos for stochastic differential equations”, *SIAM J. Scientific Comput.*, **24**(2), 619-644.
- Xu, Y.L. (2013), *Wind Effects on Cable-Supported Bridges*, John Wiley and Sons, Singapore.
- Walpole, R., Myers, R., Myers, S. and Ye, K. (2002), *Probability and Statistics for Engineers and Scientists*, 9th Ed., Upper Saddle River, NJ, USA: Pearson - Prentice Hall.
- Zhu, Z. and Gu, M. (2014), “Identification of flutter derivatives of bridge decks using CFD-based discrete-time aerodynamic models”, *Wind Struct.*, **18**(3), 215-233.